THESIS FOR THE DEGREE OF LICENTIATE OF ENGINEERING

Hydrotreatment of lignin and its bio-oils over transition metal sulfide-based supported and unsupported catalysts

You Wayne Cheah

CHALMERS

Chemical Engineering Division
Department of Chemistry and Chemical Engineering

CHALMERS UNIVERSITY OF TECHNOLOGY

Göteborg, Sweden 2021

Hydrotreatment of lignin and its bio-oils over transition metal sulfide-based supported and unsupported catalysts

You Wayne Cheah

Licentiatuppsatser vid Institutionen för Kemi och Kemiteknik
Chalmers Tekniska Högskola.
Nr 2021:08

Department of Chemistry and Chemical Engineering
Chalmers University of Technology
SE-412 96 Göteborg
Sweden
Telephone + 46 (0)31-772 1000

Cover:
Graphical illustration of the catalytic hydrotreatment of lignin to deoxygenated aromatics, cycloalkanes and phenolics over supported and unsupported transition metal sulfides.

Printed by Chalmers Reproservice
Göteborg, Sweden 2021

Hydrotreatment of lignin and its bio-oils over transition metal sulfide-based supported and unsupported catalysts

You Wayne Cheah

Department of Chemistry and Chemical Engineering
Chalmers University of Technology, Göteborg 2021

Abstract

The scarcity of fossil feedstocks and the deterioration of the current global climate condition have prompted the search for reliable alternatives for fossil fuel replacement. Biomass feedstocks such as lignin can be used to produce renewable bio-oils that can fill the gap left by fossil-derived oils. Such bio-oils require an upgrading process, such as catalytic hydrodeoxygenation (HDO), to improve their quality for use as advanced biofuels and chemicals. Transition metal sulfides (TMS) are typically used in the traditional petroleum refining industry for hydrodesulfurization (HDS) and hydrodenitrogenation (HDN) applications. This thesis focuses on the hydrotreatment of a model bio-oil compound, propylguaiacol (PG), and an actual bio-feedstock, Kraft lignin (KL), over TMS-based supported and unsupported catalysts.

In the first study, catalysts based on MoS_2 supported on γ-Al_2O_3 and promoted by transition metals, such as Nickel (Ni), Copper (Cu), Zinc (Zn), and Iron (Fe) were evaluated for the HDO of PG in a batch reactor setup. The catalyst screening results showed that the sulfided Ni-promoted catalyst gave a 94% yield of deoxygenated cycloalkanes, however, 42% of the phenolics remained in the reaction medium after 5 h for the sulfided Cu-promoted catalyst. It was also found that the sulfided Zn- and Fe-promoted catalysts gave a final yield of 19% and 16% at full PG conversion, respectively, for deoxygenated aromatics. A pseudo-first kinetic model that took into consideration the main side reactions was developed to elucidate the deoxygenation routes for the HDO of PG using sulfided catalysts. The developed kinetic model was able to describe the experimental results well with a coefficient of determination of 97% for the Ni-promoted catalyst system. This work also demonstrated that the activity of the transition metal promoters for the HDO of PG correlated to the yield of deoxygenated products from the hydrotreatment of Kraft lignin.

The main focus of the second study was on the effect of the annealing treatment of a hydrothermally synthesized unsupported MoS_2 catalyst. The prepared unsupported catalysts were studied and evaluated for the HDO of PG. The annealing treatment of the as-synthesized catalyst under N_2 flow at 400 °C for 2 h was found to enhance the HDO activity of PG. The effect on catalysts activity of hydrothermal synthesis time and acid addition combined with the annealing treatment was also studied for the same model reaction. The annealed MoS_2 with a synthesis time of 12 h in an acidic environment was found to have improved crystallinity and to exhibit the highest degree of deoxygenation of all the studied catalysts, moreover, giving a full PG conversion after 4 h and a final 4-propylbenzene selectivity of 23.4 %. An acidic environment during the synthesis was found to be crucial in facilitating the growth of MoS_2 micelles, resulting in smaller particles that affected HDO activity. The annealed unsupported MoS_2 that gave the best performance for HDO of PG was further evaluated for the hydrotreatment of KL. The annealed unsupported MoS_2 demonstrated a high capacity for deoxygenation with a selectivity of 78.6% and 20.1% for cycloalkanes and aromatics from KL, respectively. The results also indicate that a catalyst with high activity for deoxygenation and hydrogenation reactions can suppress char formation and favor a high lignin bio-oil yield.

Keywords: Advanced biofuels, Bio-oils, Pyrolysis oil, Propylguaiacol, Kraft lignin, Hydrotreatment, Transition metals, MoS_2, Unsupported TMS, Reaction network

Acknowledgments

This thesis work was carried out at the Department of Chemical Engineering and Competence Centre for Catalysis at Chalmers University of Technology, Göteborg, Sweden. The work started on the 1st of October 2018.

I would like to acknowledge the following people who have supported, encouraged, and guided me in different ways during this exciting journey of Ph.D. studies:

My supervisors: Prof. Louise Olsson and Prof. Derek Creaser. I would like to express my sincerest appreciation to them for believing in me and allowing me to work in this interesting field. I thank you for all your guidance and supervision during my work. And for always being so supportive and positive in every aspect of our discussions.

Olov from Preem AB: I am thankful to have you as my co-supervisor. Your knowledge in the field and also all our discussions from the industrial point of view were extremely appreciated. I enjoyed our discussion during all the project meetings and I very much look forward to more of the same. Thanks.

I am also thankful to Linda and Niklas from RISE ETC for all the interesting discussions during the project meeting. I look forward to our future collaboration!

Salam, thanks for all the help and guidance in the lab and also all the interesting discussions during our work. I thank you!

Prakhar, whom I met briefly before I started my work in Göteborg, turned out to be one of my good friends outside of work and a good teacher at work. I cherished our discussions on various subjects. Thank you.

All postdocs in the lab. Specially thanks to Sreetama, Poonam, Joby, and Phuoc for all your guidance in my research. Your willingness to teach and guide is something that I appreciate.

All past and present colleagues in KCK, SIKT, and Chemical Engineering, thanks for making Chalmers a good working place.

At last, I would like to dedicate this work to my family for always giving me the complete freedom to pursue what I enjoy.

You Wayne

March 2021, Göteborg

This project is a collaboration between the Competence Centre for Catalysis, Chemical Engineering at Chalmers, Preem AB, and RISE Energy Technology Centre (ETC). We would like to acknowledge the Swedish Energy Agency (2017-010890) and Preem AB for research funding. The Competence Centre for Catalysis is hosted by the Chalmers University of Technology and financially supported by the Swedish Energy Agency and member companies AB Volvo, ECAPS AB, Johnson Matthey AB, Preem AB, Scania CV AB, and Umicore Denmark ApS. We would also like to acknowledge Chalmers Material Analysis Laboratory (CMAL) for SEM, TEM, XPS, and XRD analysis.

List of publications

This thesis is based on the following appended papers:

I: Role of transition metals on MoS_2-based supported catalysts for hydrodeoxygenation (HDO) of Propylguaiacol.

You Wayne Cheah, Muhammad Abdus Salam, Prakhar Arora, Olov Öhrman, Derek Creaser, and Louise Olsson

Sustainable Energy and Fuels, 2021, **5**, 2097-2113 (https://doi.org/10.1039/D1SE00184A)

Contribution: I planned and defined the scope of the study with co-authors. I performed all the experiments in this work. I analyzed the results with co-authors and wrote the manuscript. I revised the manuscript with feedback from co-authors.

II: Thermal annealing effects on hydrothermally synthesized unsupported MoS_2 for enhanced deoxygenation of Propylguaiacol and Kraft lignin

You Wayne Cheah, Muhammad Abdus Salam, Joby Sebastion, Sreetama Ghosh, Olov Öhrman, Derek Creaser, and Louise Olsson

Submitted.

Contribution: I planned and defined the scope of the study with co-authors. I performed all the experiments in this work. I analyzed the results with co-authors and wrote the manuscript. I revised the manuscript with feedback from co-authors.

Publications not included in this thesis

I: NiMoS on alumina-USY zeolite for hydrotreating lignin dimers: Effect of support acidity and cleavage of C-C bond

Muhammad Abdus Salam, Prakhar Arora, Houman Ojagh, **You Wayne Cheah**, Louise Olsson, and Derek Creaser

Sustainable Energy and Fuels, 2020, **4**, 149-163 (https://doi.org/10.1039/C9SE00507B)

II: The role of catalyst poisons during hydrodeoxygenation of renewable oils

Prakhar Arora, Hoda Abdolahi, **You Wayne Cheah**, Muhammad Abdus Salam, Eva Lind Grennfelt, Henrik Rådberg, Derek Creaser, and Louise Olsson

Catalysis Today, 367 (2021) 28-42 (https://doi.org/10.1016/j.cattod.2020.10.026)

List of abbreviations

AC	Activated carbon
BJH	Barret Joyner Halenda
BET	Brunauer Emmett Teller
BDE	Bond dissociation energy
DME	Demethylation
DDO	Direct-deoxygenation
DMO	Demethoxylation
DMDS	Dimethyl disulfide
EDX	Energy dispersive x-ray
FID	Flame ionization detector
GC	Gas chromatography
GHG	Greenhouse gas
HAADF	High angle annular dark field
HDO	Hydrodeoxygenation
HDS	Hydrodesulfurization
HDN	Hydrodenitrogenation
HDM	Hydrodemetallization
HYD	Hydrogenation-dehydration
HRTEM	High-resolution transmission electron microscopy
ICP-SFMS	Inductively coupled plasma sector field mass spectrometry
kDa	Kilodaltons
MS	Mass spectroscopy
MTOE	Million tons of oil equivalent
ODE	Ordinary differential equations
RPM	Revolutions per minute
SSR	Residual sum of squares
SEM	Scanning electron microscopy
STEM	Scanning transmission electron microscopy
TMS	Transition metal sulfides
TIA	TEM Imaging and Analysis
XRD	X-ray diffraction
XPS	X-ray photoelectron spectroscopy

Contents

1 Introduction

1.1 Greenhouse gases (GHG) emissions, the transportation sector in Europe, and biofuels

Depleting fossil resources, increasing greenhouse gases (GHG) emissions, and deteriorating global climate conditions have prompted efforts to speed up the deployment of a sustainable society. Several aspiring goals have been set by governmental agencies to tackle these issues and environmental-related issues. One of these is the ambitious target to reduce greenhouse gas (GHG) emissions by 40% in 2030 and achieve climate neutrality by 2050, as drafted in the roadmap of the European Green Deal illustrated in Figure 1[1]. 23.2% lower emissions of GHGs were achieved in 2018 than in 1990, indicating that the EU remained on track in its goal of a 20% reduction in GHG emissions by 2020 (Figure 1)[1]. However, extensive efforts are still needed to halt GHG emissions and gain carbon neutrality.

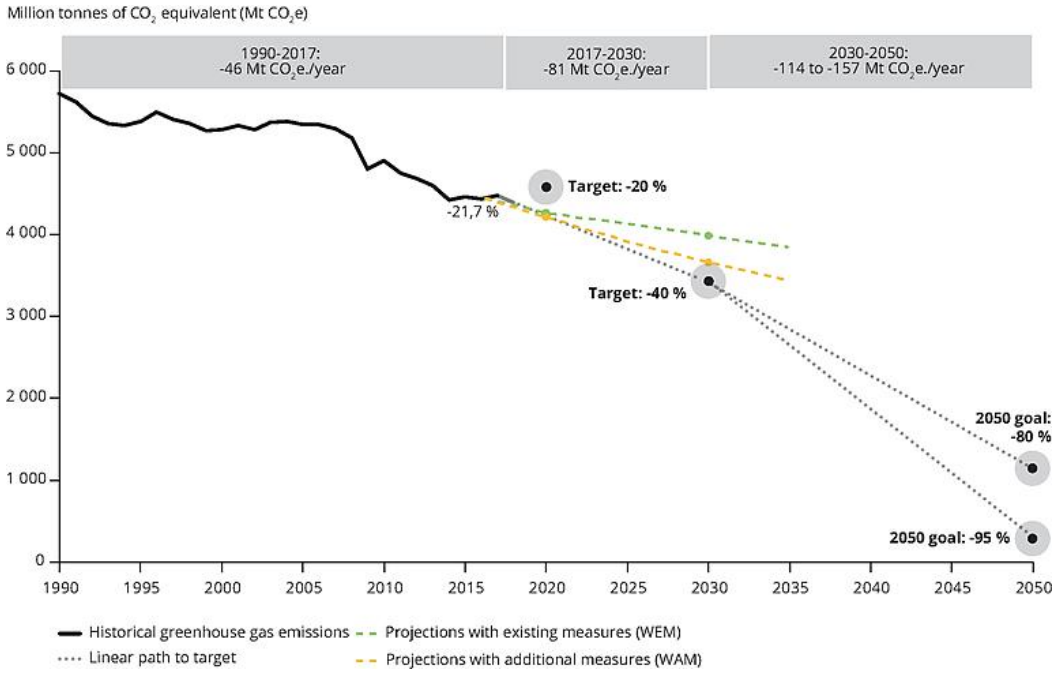

Figure 1. GHG emission trends, projections, and targets in EU[1].

Of all the economic sectors, transportation accounts for almost a quarter of the GHG emissions in Europe, which also causes air pollution in major cities[2]. The transport sector also remains as one of the major economic sectors with an upward trend for GHG emissions, i.e., 29% above 1990 levels for 2018 (Figure 2)[2]. This increase can be mainly attributed to the ever-growing population and demand for passenger and freight transport in emerging economies. The current billion-vehicle fleet in the transport sector is still largely dependent on using fossil-derived liquid hydrocarbons, e.g., diesel, gasoline, kerosene with growing demand especially in aviation and marine transport. Consequently, sustainable biofuels play a significant role in decarbonizing the transport sector and shifting towards a fossil-free society.

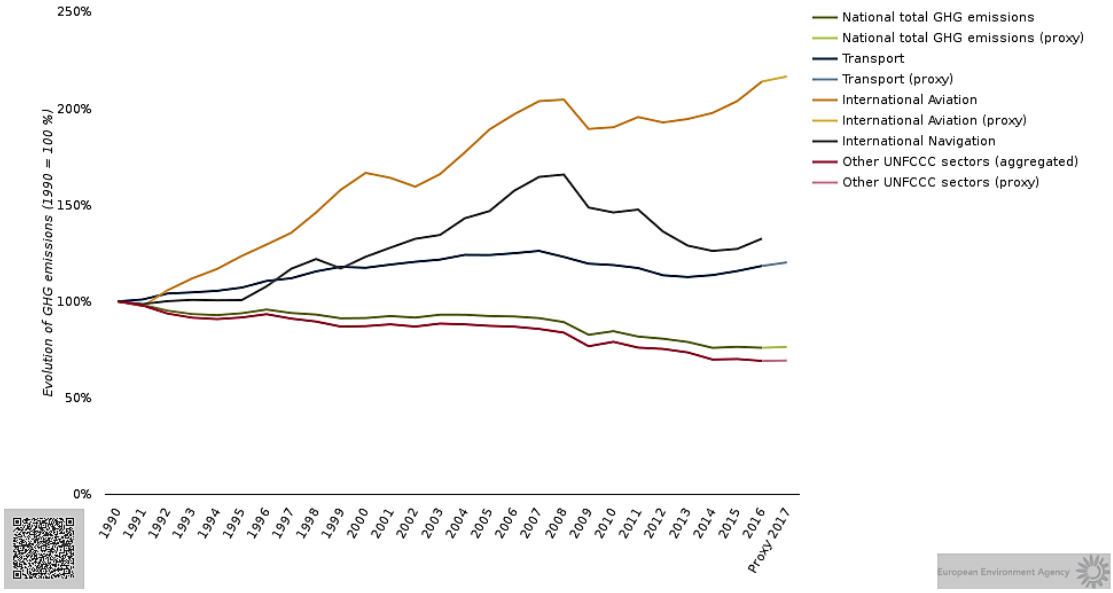

Figure 2. EU GHG in the transport sector[2].

Biofuels are renewable energy sources derived from biomass. There are typically three types of biofuels: the first, second, and third-generation biofuels are characterized based on the biomass feedstocks used during the production process and their limitations as an energy source. The first-generation biofuels are derived from food crops such as sugar beets, corn starch, or vegetable oils. They are produced through well-understood processes such as fermentation, distillation, and transesterification. However, these feedstocks are criticized for competing with food crops, which impact biodiversity and the competition for water. The production of second-generation biofuels was initiated to address the various disadvantages and limitations of first-generation biofuels. The second-generation biofuels use non-edible feedstocks from waste streams, e.g., food waste and agricultural waste. These feedstocks can undergo different processes, such as thermochemical conversion (pyrolysis, gasification, liquefaction, and direct combustion), biochemical conversion, and hydroprocessing, and yield renewable fuels. The production of bio-diesel from the hydroprocessing of vegetable oils (HVO) and esters and fatty acids (HEFA) are great examples that fall under this category. The third-generation biofuels mainly use engineered crops, such as algae biomass, which have a different growth yield in comparison to the typical lignocellulosic biomass.

1.2 Objectives, scope, and outline of the thesis

Lignocellulosic biomass-derived bio-oils produced via the thermochemical conversion of solid biomass and further upgrading through catalytic hydrotreatment have gained tremendous attention as a substitute for fossil-derived fuels in recent years. This two-stage process was drawn and shown in Scheme 1. These biomass-derived oils from for example fast pyrolysis are also known as pyrolysis oil. Pyrolysis oil has a water content of 15-30 wt% and a high oxygen content which contributes to its poor quality and also makes its utilization as fuel in internal combustion engines difficult. Hence, catalytic hydrotreatment, the second stage as shown in Scheme 1 is required to refine the biomass-derived bio-oils so that they can be used as liquid transportation fuels.

Of the different biomass conversion technologies and upgrading processes, catalytic HDO remains an interesting subject to study for the improvement of the quality of biomass-derived bio-oils for direct use as transportation fuels. The main challenges of the complex HDO reaction of biomass-derived bio-oils are catalyst development,

catalyst stability and poisoning, reaction mechanisms, and network elucidation. Therefore, in this work, the focus has been placed on the main upgrading process, catalytic hydrodeoxygenation of a bio-oil model compound as illustrated in the 2nd-step in Scheme 1 to produce deoxygenated aromatics, cycloalkanes, and alkylphenols. Moreover, biorefinery waste such as Kraft lignin provides an alternative to fossil feedstocks for the production of renewable chemicals and fuels. Thus, the simultaneous depolymerization and hydrodeoxygenation of Kraft lignin in the presence of a solvent in one step was also investigated, as shown in Scheme 2. The current work provides a potential strategy for an efficient one-step valorization of the waste stream into high-value chemicals, platform chemicals, and liquid fuels.

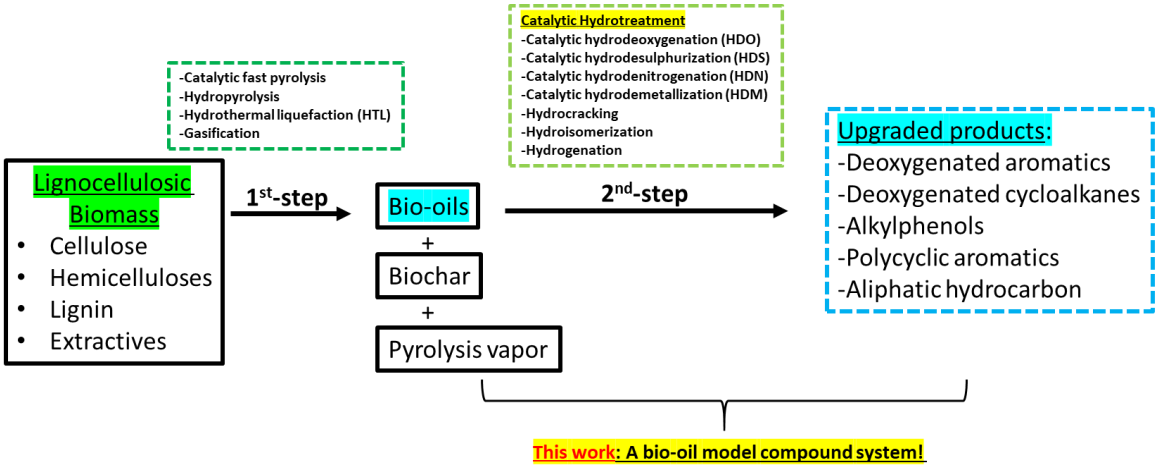

Scheme 1. Two-stage process in the transformation of raw biomass to valuable products such as chemicals and transportation fuels.

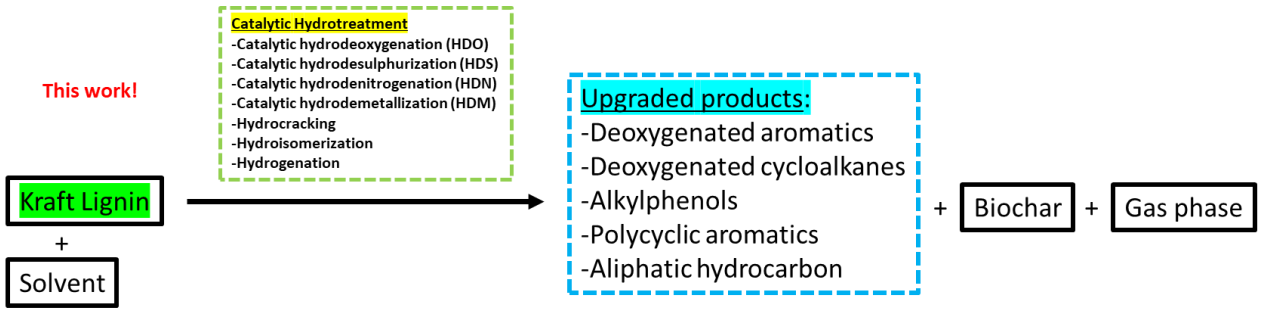

Scheme 2. One-step hydrotreatment of Kraft lignin in the presence of a solvent for the production of high-value chemical and fuel components.

The main effort has been placed on investigating different transition metal sulfides (TMS), with and without catalyst support in the HDO of a bio-oil model compound, propylguaiacol (PG). The activity and selectivity of the sulfided catalysts for different desired products, such as deoxygenated aromatics, cycloalkanes, and alkylphenolics, were studied. A series of screening experiments were conducted in the first study to examine the Ni, Fe, Zn, and Cu on the Mo-based sulfided catalysts for the HDO of PG. The effect of these transition metals was studied and compared with the traditional NiMo sulfided catalysts. All catalysts were subjected to different characterization techniques, such as X-ray diffraction (XRD), inductively coupled plasma (ICP)-sector field mass spectroscopy, nitrogen physisorption (BET), X-ray photoelectron spectroscopy (XPS), and transmission electron

microscopy (TEM). A simplistic pseudo-first-order kinetic model that took into consideration side reactions was developed based on the proposed reaction network for HDO of PG over sulfided catalysts. Sulfided ZnMo, FeMo, and NiMo catalysts were also examined in the hydrotreatment of Kraft lignin, and the product selectivities were correlated with the results obtained from the HDO of PG.

The synthesis of unsupported MoS_2 catalysts using a facile hydrothermal synthesis method was examined in the second study. The effect of annealing treatment on the unsupported catalysts was studied in the HDO of PG. The combined effect of hydrothermal synthesis time and pH adjustment during the synthesis with the annealing treatment were investigated. Our in-house synthesized unsupported MoS_2 was compared with a sample of bulk MoS_2 in the model reaction and hydrotreatment of Kraft lignin.

The outline of this thesis is as follows:

Chapter 2 introduces the background of lignin, biomass-derived bio-oils, and catalytic hydrodeoxygenation (HDO). The same chapter also presents an extensive literature review on the HDO of phenolic monomers and real biomass feedstocks using supported and unsupported sulfided catalysts. The motivation for conducting studies using supported and unsupported sulfided catalysts is discussed.

Chapter 3 presents the experimental techniques used in catalyst synthesis, catalyst testing experiments, and the catalyst characterizations involved in both studies.

Chapter 4 presents the main findings and a discussion of both studies.

Chapter 5 provides the conclusion and summary of both studies.

Chapter 6 discusses future work

2 Background

2.1 Lignin, bio-oil properties, and catalytic hydrodeoxygenation (HDO)

Lignocellulosic biomass, one of the most abundant renewable resources on Earth has gained great interest in replacing fossil feedstock as a major source of renewable carbon. It can play a vital role in the production of renewable carbon-based chemicals, materials, and fuels. The major mass of lignocellulosic biomass is found in the wood/plant cell wall which mainly consists of three biopolymers: cellulose (40-50%), hemicellulose (25-40%), and lignin (20-30%), and also extractives. The composition of biomass largely depends on the biomass species. The fibers in the middle lamella and the bundled fibrils are bounded together by hemicellulose and lignin that give the tree and the wood its mechanical strength. Lignin is essentially comprised of phenylpropane units, such as coniferyl, sinapyl, and p-coumaryl alcohol (Figure 3b) which are randomly interlinked by recalcitrant C-C and C-O bonds, as shown in Figure 3a[3]. In the pulp and paper industry, lignin is a byproduct that has been often used as a renewable energy source by burning it to produce heat and energy for the paper mill and also to recover the inorganics. However, modern paper mills are increasingly energy-efficient, which has resulted in the energy from lignin combustion becoming unnecessary for the operation of the mill[4]. Due to the increasing demand for a renewable carbon source in the production of biofuels and green chemicals, much research attention has been given to the efficient valorization of waste lignin into valuable chemicals and fuel components.

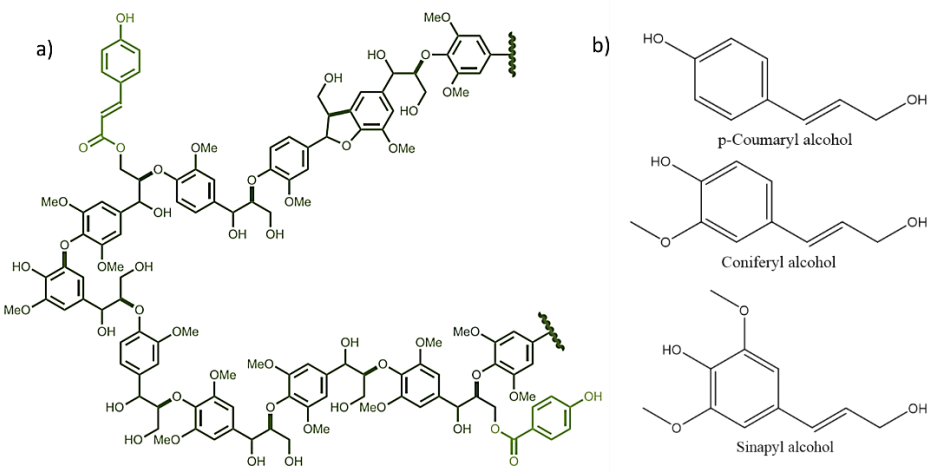

Figure 3. a) Model lignin chemical structure and b) building blocks of lignin.

Bio-oils can be produced via various processes and one of which is fast pyrolysis or thermal liquefaction of biomass[5]. Fast pyrolysis is a thermochemical process where biomass is decomposed into bio-oils, bio-char, and volatile species at temperatures between 300-600 °C in the absence of oxygen with a short residence time of less than 2 s[6]. The chemical composition of bio-oils can vary depending on the difference in the biomass feedstock used and the pyrolysis conditions. Different compound groups, such as acids, alcohols, aldehydes, ketones, phenolics, sugars, can be found in bio-oil constituents[6]. This pool of compounds is derived from the depolymerized cellulose, hemicellulose, and lignin fraction of the lignocellulosic biomass. This liquid product also has a high-water content (15-30 wt%), which comes from the initial moisture of the biomass and is acidic (pH 2-4) in nature

due to the presence of carboxylic acids[6]. The oxygen content of this product is also high which can contain up to 40 wt% oxygen giving high viscosity and a low heating value in comparison to fossil-derived hydrocarbon fuels[6].

Biomass-derived bio-oils have various undesirable properties, leading to difficulties for their direct use as transportation fuels. Hence, bio-oils require a refining process to produce deoxygenated products that are compatible with existing fuel grades. Catalytic hydrotreating is a conventional hydroprocessing technology employed by refineries to improve the quality of fuels. This technology removes heteroatoms, such as sulfur, nitrogen, oxygen, and metals from the fossil feedstock through hydrodesulfurization (HDS), hydrodenitrogenation (HDN), hydrodeoxygenation (HDO), and hydrodemetallization (HDM). Bio-oils are different from petroleum oil, because they typically have a negligible content of sulfur and nitrogen, whereas bio-oils have a high oxygen content. Hence, catalytic hydrodeoxygenation (HDO) has been adopted to remove excess oxygen from the bio-feedstocks in the form of water while using hydrogen as a co-reactant with the aid of a selective hydrotreating catalyst[7]. Different reactions, such as demethoxylation (C-OCH_3 cleavage), dehydroxylation (C-OH cleavage), hydrogenation (C=O and aromatic ring saturation), hydrogenolysis, hydrocracking, transalkylation, and isomerization can occur at varying degrees during HDO, depending on the composition of the bio-oil, the reaction conditions and the catalyst used.

There has been great interest in studying the reaction networks and kinetics of the HDO of bio-oils over the past decades due to the increased utilization of such feedstocks for renewable fuel production. However, due to the complexity of the nature of bio-oils, several reactions can occur simultaneously during the upgrading process. Therefore, much research has been dedicated to the study of bio-oil model compounds in a lab-scale reactor to understand the reaction network and reaction mechanism for HDO. The use of model compounds allows a quick assessment of the catalyst's activity and selectivity for compound groups, such as alkylphenols, deoxygenated cycloalkanes, and aromatics, before diving into complex feedstocks like lignin and pyrolysis oils. Different functional groups in the model compounds also facilitate the understanding of the relative activities and selectivity of the catalysts in cleaving different bonds and linkages. Table 1 provides the bond dissociation energies (BDE) for different types of C-O bonds in bio-oil-derived model compounds[8]. There are typically three types of C-O bonds: the bond between $C_{aromatic}$-OH (Ph-OH), $C_{aromatic}$-OCH_3 (Ph-OMe), and $C_{aromatic}$-O-CH_3 (Ph-O-Me) or $C_{aromatic}$-O-$C_{aromatic}$ (Ph-O-Ph). The BDE analysis shows that the C-O bond energies decreased in the order: Ph-OH > Ph-OMe > Ph-O-Ph > Ph-O-Me. The etheric C-O bond is also weaker than the phenolic C-O bond.

In this thesis, the focus is on the HDO of the bio-oil model compound, 4-propylguaiacol (PG), and the hydrotreatment of Kraft lignin (KL). The selection of PG as a model bio-oil compound is because PG has a similar structure to coniferyl alcohol present in the lignin structure. The application of traditional transition metal sulfides (TMS) with and without catalyst support on the model reaction was investigated to understand the reaction network and kinetics of the HDO of PG.

Table 1. The calculated homolytic bond dissociation energies (BDE) for different bio-oil model compounds calculated with B3lyp/6-311 G(d,p) level theory at 320 °C in the gas phase adapted from reference[8]. The unit for BDE is given in kJ/mol.

Bond	Ph-OH	Ph-OMe	Ph-O-Me	Ph-O-OH
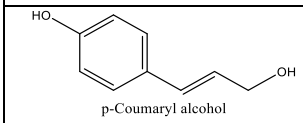 p-Coumaryl alcohol	446.4	-	-	-
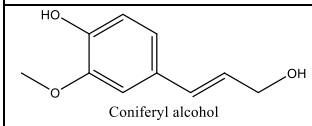 Coniferyl alcohol	440.2	379.5	226.8	-
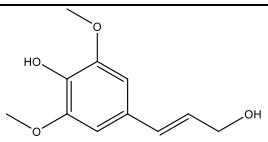 Sinapyl alcohol	453.5	384.5	214.2	-
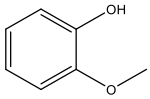 Guaiacol	456.8	397.0	205.0	-
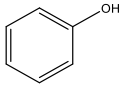 Phenol	443.9	-	-	-
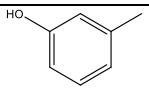 m-cresol	443.5	-	-	-
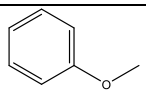 Anisole	-	384.0	238.0	-
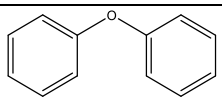 Diphenyl Ether	-	-	-	291.6

2.2 Transition metal sulfides for HDO process

The catalytic performance and progression of different reactions during HDO depend largely on the catalyst types, the catalyst support used, and HDO reaction conditions (reactor type, temperature, reaction time, solvent system, and pressure). Traditional transition metal sulfide (TMS) catalysts are usually employed in HDS and HDN. The conventional catalyst systems used are the typical molybdenum or tungsten sulfide systems supported on alumina promoted by nickel (Ni) or cobalt (Co). TMS catalysts must be kept in sulfide form, and sulfiding agents, such as dimethyl disulfide (DMDS) or carbon disulfide (CS_2) are commonly co-fed in the HDO reactions on a lab-scale to maintain the sulfidation degree of the catalysts.

There are many reports related to the use of alumina as a support for hydrotreating catalysts because of its good textural and mechanical properties, and the fact that it is relatively inexpensive[9,10]. The acidic properties of alumina

are known to be beneficial in breaking the C-O bond in anisole which can be found in lignin oil[9]. The effect of different supports such as silica, activated carbon, and alumina on the activity of NiMo hydrotreating catalyst was also studied in vacuum residue hydrotreating reactions[10]. They concluded that the effectiveness of a hydrotreating catalyst depends largely on the size of the pore diameter, pore volume, and also the dispersion of the active metals that can contribute to a better hydroconversion[10]. This indeed highlights the importance of using support materials for the synthesis of hydrotreating catalysts. Mukundan et. al also studied the use of carbon support for MoS_2-based catalysts and found promising results for HDO reactions[11,12]. Carbon as catalyst support attracts interest for HDO reactions because of its high surface area, inert nature, high thermal stability, stability in water, and low cost[13].

Other than supported TMS catalysts widely reported in literature studies, many works have also been dedicated to the exploration of the potential of using unsupported TMS catalysts for hydroprocessing. The use of unsupported TMS catalysts allows for the direct use of the main active phase of the catalyst and eliminates any possible interference of the support material during the reaction. One excellent example of the use of an unsupported catalyst system is the NEBULA technology that has been jointly established by ExxonMobil and Albemarle Catalysts[14,15]. This commercialized and patented technology has been able to show the superior activity of the unsupported catalysts as compared to the conventional hydroprocessing catalysts[15]. Another application of the unsupported hydroprocessing catalysts was the Eni Slurry Technology (EST) process[16]. The EST process uses highly dispersed MoS_2 nanoparticles formed by the oleo-soluble molybdenum precursor co-feeded with heavy oil feedstocks under reaction conditions of 400-450 °C and 150 bar with a continuous hydrogen flow resulting in high hydrogenation activity[16]. Furthermore, the promising results were demonstrated in a recent study using unsupported Mo precursors for the co-processing of fast pyrolysis bio-oil (FPBO) with heavy fossil feedstocks in a slurry hydrocracking unit[17].

In this work, Kraft lignin was used as a renewable feedstock in the hydrotreatment process. Kraft lignin has a high molecular weight of typically around 16.7 kDa[18]. Hence, there is a significant obstacle for the diffusion of such large lignin polymer molecules or even their fragments into the porous support of the catalytic materials to access active sites. Besides, depolymerized lignin fragments produced from non-catalytic reactions can repolymerize and form char[19,20]. Therefore, the transport limitations caused by the catalyst supports can hinder the stabilization of these radicals through hydrogenation reactions and promote char production. In this context, the use of highly active unsupported catalysts became attractive when dealing with lignin hydrotreatment. Moreover, Kraft lignin contains 1-2 wt% sulfur due to the pulping process and the sulfur content may act as a poison to noble metal catalyst systems[21]. Therefore, the use of sulfur tolerant catalysts like TMS can be of advantage when applied to the Kraft lignin hydrotreatment.

Sections 2.3, **2.4**, and **2.5** discuss the application of traditional supported and unsupported HDS catalysts in the upgrading of bio-oil monomer phenolics and biomass feedstocks with emphasis on reaction mechanism and networks.

2.3 HDO of bio-oil model compounds over supported sulfided catalysts

Table 2 presents the state of the art of supported sulfided catalysts for hydrotreating of phenolic monomers. Various catalytic systems employing mixed oxide support in sulfided catalysts have been reported for the HDO of phenolics. Garcia-Mendoza et al. have studied the activities of NiWS supported on TiO_2, ZrO_2, and the mixed

oxide TiO_2-ZrO_2 for the HDO of Guaiacol at 320 °C[22]. Their results show that the support was responsible for the HDO reaction producing phenol, catechol, and methylated compounds with NiWS supported on TiO_2 showing an 80% HDO product selectivity at full guaiacol conversion[22]. In a similar catalyst system, Hong et al. have shown that a 2 wt% Ni loading and 12 wt% W loading on such mixed oxide sulfided catalysts can give full guaiacol conversion and a 16% cyclohexane yield in different reaction conditions[23]. The study also mentions that nickel (Ni) performs better than cobalt (Co) as a promoter in catalyzing the HDO of guaiacol[23]. Another study using CoMoS supported on the mixed oxide Al_2O_3-TiO_2 for the HDO of phenol has also shown that the mixed oxide improved the HDO activity with a better metal-support interaction than the conventional CoMoS supported on Al_2O_3[24]. The use of activated carbon as catalyst support has also been reported in the literature[25–27]. Mukundan et al. have prepared a single-layered amorphous MoS_2 on activated carbon for the HDO of guaiacol and found that single-layer MoS_2 promotes deoxygenation and hydrogenation better than multi-layered MoS_2 in the production of phenol[27].

The traditional NiMo on γ-Al_2O_3 in sulfided and reduced form was studied for phenol HDO[28]. Figure 4 shows general reaction networks for the HDO of phenol using a sulfided NiMo catalyst[28]. The catalyst in sulfided form exhibited a higher than 90% cyclohexane selectivity, and the deoxygenation routes for the phenol HDO occurred in parallel, involving direct deoxygenation (DDO) of the hydroxyl group of phenol and the hydrogenation-dehydration (HYD) of the phenyl ring[28]. The promoters play a role in conventional hydroprocessing catalysts. Badawi et al. have demonstrated that cobalt promotes both DDO and HYD pathways in the HDO of phenol to different extents[29]. They have performed DFT calculation and shown that both DDO and HYD pathways occur on sulfur vacancy sites (CUS)[29]. Romero et. al have also reported the same findings[30]. Using 2-ethylphenol as a model compound[30], they have found that both Ni and Co improve the deoxygenation rate, while Ni only facilitates the HYD pathway. The reaction mechanism for DDO and HYD is illustrated in Figure 5 and Figure 6, respectively[30].

In addition to Ni and Co, a study conducted by Yang et al. has demonstrated that phosphorus (P) was able to promote the phenol HDO activity over a CoMoS-supported MgO catalyst, and they proved that DDO is the major pathway in phenol deoxygenation[31]. A non-conventional hydrotreating catalyst like supported ReS_2 has been reported in several studies[32–36]. For instance, ReS_2 supported on SiO_2 or γ-Al_2O_3 catalyst was applied in the coprocessing of dimethyl dibenzothiophene and guaiacol[36]. Both Re-based catalysts showed high HDS and HDO activities; ReS_2 supported on SiO_2 catalyst showed high HDO rates giving 40% HDO products[36]. In addition to the cheap transition metals used as promoters, research has examined the use of noble metals as promoters for a metal sulfide catalyst in phenolics HDO[33,37]. For instance, Ir and Pt have been incorporated into RuS_2/SBA-15 and used in the HDO of phenol[37]. The results have demonstrated a higher conversion rate of phenol (37-41%) and better cyclohexane selectivity (62-63%) than the non-promoted RuS_2/SBA-15[37]. It is important to note that the use of noble metals involves high costs for catalyst production, which limits their industrial application. The sulfur content in bio-feedstock, such as Kraft lignin, may act as a poison to such noble catalyst systems, nevertheless, studying such a system facilitates better insight into the reaction pathways of the HDO of phenolics.

Jongerius et al. have studied a pool of lignin model compounds using CoMoS supported on Al_2O_3 under the same reaction parameters (300 °C, 50 bar H_2, 4 h, and batch system) for comparison[38]. Their main findings suggest that the mono-aromatic oxygenates underwent three distinct pathways that included HDO, demethylation, and methylation. This resulted in invaluable products like phenol, benzene, cresols, and toluene[38]. Less than 5% of

hydrogenated products were detected in the reaction medium, indicating that hydrogenation is the least preferred reaction network for this catalyst system[38].

It is commonly found in the considerable amount of studies on the HDO of phenolic compounds that sulfiding agents, such as dimethyl disulfide (DMDS) or carbon disulfide (CS_2), were co-fed during an experiment to create H_2S to maintain the sulfidation degree of the sulfided catalyst. Results show that adding a sulfiding agent during the HDO process had a negative effect on the HDO activity of phenolics but promoted the HDO of aliphatic oxygenates such as vegetable oils and animal fats[39]. However, one should notice the addition of a sulfiding agent also plays a role in affecting the effectiveness of the catalyst other than the type of reactant being used. Ferrari et al. have studied the effect of H_2S partial pressure and sulfidation temperature on the conversion and selectivities of phenolics[25]. It was found that the increase in H_2S partial pressure reduced the formation of deoxygenated products from the HDO of guaiacol over CoMoS supported on carbon[25].

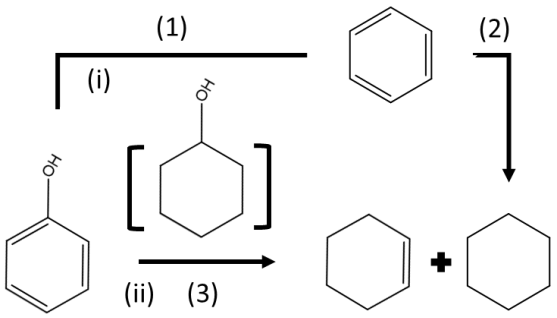

Figure 4. Reaction scheme for phenol HDO over sulfide supported NiMo catalyst[28]. Reprinted (adapted) with permission from Templis, C. C, Revelas, C. J, Papastylianou, A. A, Papayannakos, N. G., *Ind. Eng. Chem. Res*., 2019, 58 (16), 6278-6287. Copyright (2019) American Chemical Society.

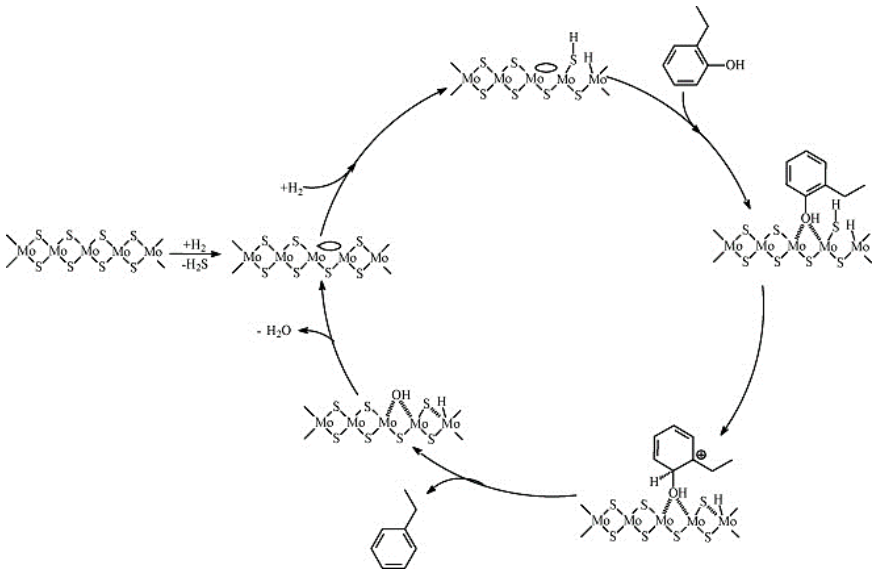

Figure 5. DDO reaction pathway for HDO of 2-ethylphenol over supported MoS_2 catalysts[30]. This article was published in *Applied Catalysis B: Environmental*, Y. Romero, F. Richard, and S. Brunet, Hydrodeoxygenation of 2-Ethylphenol as a Model Compound of Bio-Crude over Sulfided Mo-Based Catalysts: Promoting Effect and Reaction Mechanism, *Appl. Catal. B Environ*., 2010, 98 (3-4), 213–223, Copyright Elsevier (2010).

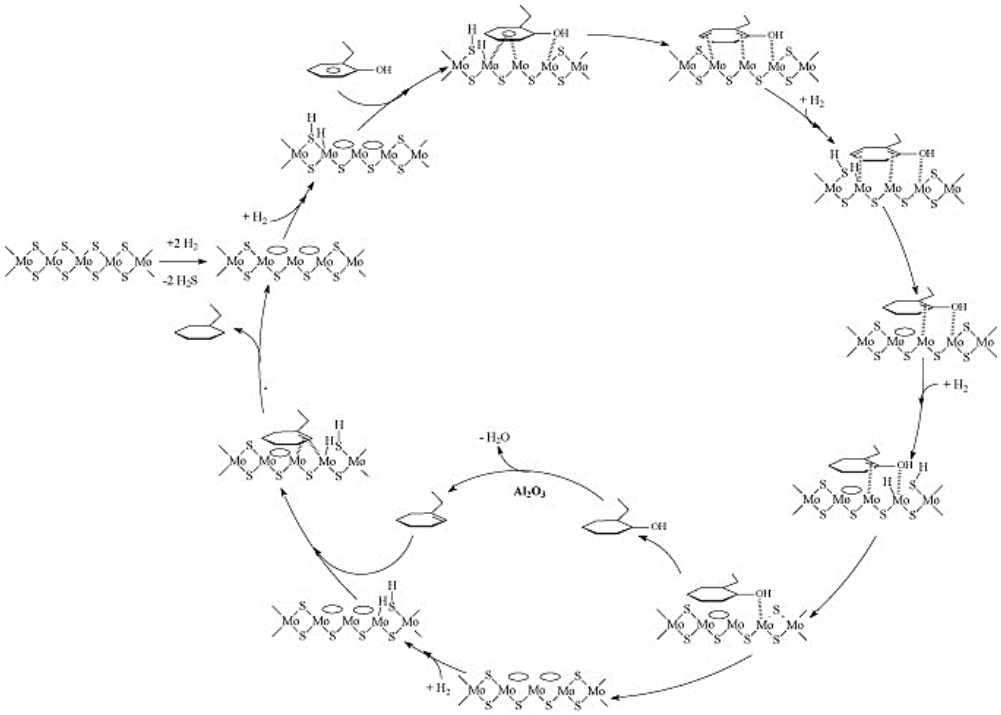

Figure 6. HYD reaction pathway for HDO of 2-ethylphenol over supported MoS_2 catalysts[30]. This article was published in Applied Catalysis B: Environmental, Y. Romero, F. Richard, and S. Brunet, Hydrodeoxygenation of 2-Ethylphenol as a Model Compound of Bio-Crude over Sulfided Mo-Based Catalysts: Promoting Effect and Reaction Mechanism, Appl. Catal. B Environ., 2010, 98(3-4), 213–223, Copyright Elsevier (2010).

Table 2. State-of-the-art sulfided supported catalysts for HDO of phenolic oxygenates.

Entry	Sulfided catalyst	Model compound	Solvent	Conversion (%)	Reaction conditions	HDO product selectivity (%)	Ref.
1	NiWS supported on TiO_2, ZrO_2, and TiO_2-ZrO_2	Guaiacol	Hexadecane	100	Batch, 320 °C, 55 bar H_2, and 1000 rpm	80% cycloalkanes (NiWS-TiO_2)	[22]
2	CoMoS supported on Al_2O_3-TiO_2	Phenol	Dodecane	93	Batch, 300 °C, 54 bar H_2, and 1000 rpm	Benzene (65%), Cyclohexane (25%) and Cyclohexene (3%)	[24]
3	NiWS supported on TiO_2	Guaiacol	n-decane	100	Batch, 2.5 h, 300 °C and, 70 bar	Phenol (37%), Cyclohexane (16%), Benzene (1%), Creasol (3%) and others (43%)	[23]
4	NiMoS supported on γ-Al_2O_3	Phenol	Dodecane	-	Continuous, WHSV = 29/ 36 h^{-1}, 200/ 220/ 250 °C and 30 bar	Cyclohexene (traces), Cyclohexane (93.4%) and benzene (6.5%) for 200 °C and 29 h^{-1}	[28]
5	CoMoS supported on Al_2O_3	Phenol/2-ethylphenol	Toluene	-	Continuous, 400 °C, 70 bar	HDO activity (29.1 $mmol.h^{-1}g^{-1}$) for phenol and (22 $mmol.h^{-1}g^{-1}$) for 2-ethylphenol	[29]
6	NiMoS/CoMoS supported on γ-Al_2O_3	Guaiacol/Phenol	m-xylene /n-hexadecane	30-100	Continuous/batch, 200-350 °C, 75-80 bar	Cycloalkanes (55% for NiMo and 45% for CoMo) at 300 °C	[40]
7	CoMoS supported on Al_2O_3	Phenol, o-cresol, anisole, 4-methylanisole,	Dodecane	25-90	Batch, 4 h, 300 °C and, 50 bar	See ref [38]	[38]

		catechol, guaiacol, 4-methylguaiacol, 1,3-dimethoxybenzene, syringol, and vanillin.					
8	NiMoS supported on γ-Al_2O_3	Phenol and methyl heptanoate	Dodecane	100	Batch, 200/250 °C, and 75 bar	Cyclohexane (85%), cyclohexyl cyclohexane (14%), and others (1%)	[41]
9	MoS_2/NiMoS/CoMoS supported on Al_2O_3	2-ethylphenol	Toluene	22-24	Continuous, 340 °C, and 70 bar	Oxygenated compounds (19.1%) and deoxygenated compounds (80.9%) for NiMoS	[30]
10	CoMoP/MgO	Phenol	Supercritical hexane	17-90	Batch, 350-450 °C, 1 h and 50 bar	Benzene (65%) and other (26%) at 450 °C	[31]
11	NiMoS/CoMoS supported on γ-Al_2O_3	Phenol and methyl heptanoate	m-xylene	5-28	Batch/continuous, 250 °C, 1 h and 15 bar	See ref[39]	[39]
12	CoMoS supported on Al_2O_3	Methyl-substituted phenols	n-heptane/n-decane	10-50	Continuous, 300 °C and 28.5 bar	See ref[42]	[42]
13	CoMoS on activated carbon	Guaiacol, ethyldecanoate, and 4-methylacetophenone	-	17-19	Continuous, 270 °C and 75 bar	See ref[25]	[25]
14	MoS_2 on activated carbon	Guaiacol	Decalin	10-30	Batch, 300 °C, 50 bar, and 1000 rpm	See ref[26]	[26]
15	MoS_2 on activated carbon	Guaiacol	Dodecane	55	Batch, 300 °C, 50 bar, 5 h, and 1000 rpm	Phenol (52%), Cycloalkanes (12.2%), cyclohexanol (5%), anisole (0.3%), benzene (0.4%), catechol (1.8%), veratrole (0.8%), methanol (0.04%) and gases.	[27]
16	(Ir or Pt) RuS_2/SBA-15	Phenol	Decalin	37-41	Continuous, WHSV = 1.28 h^{-1}, 310 °C, 30 bar, and TOS = 4 h	For Ir-RuS_2/SBA-15, cyclohexane (63%), cyclohexene (11%), benzene (7%), and cyclohexanol (19%)	[37]
17	ReS_2/SiO_2	Guaiacol and phenol	Hexadecane and dodecane	15-20	Batch, 250 °C, 50 bar, and 4 h	For guaiacol, phenol (13%), catechol (1%), and cyclohexanol (0.5%)	[33]
27	ReS_2/SiO_2	Guaiacol	Dodecane	80	Batch, 300 °C, 50 bar, and 4 h	For ReS_2/SiO_2, phenol (60%), cyclohexane (20%) and others.	[32]
28	ReS_2/activated carbon	Guaiacol	Dodecane	40-80	Batch, 300 °C, 50 bar, and 4 h	See ref[34]	[34]
29	$ReS_2/SiO_2(Al_2O_3)$	Guaiacol and 4,6-dimethyldibenzothiophene	Dodecane	80	Batch, 300 °C, 50 bar, and 4 h	See ref[36]	[36]
30	Re/ZrO_2 and Re/ZrO_2-sulphated	Guaiacol	Decaline	10-70	Batch, 300 °C, 50 bar, and 4 h	See ref[35]	[35]

2.4 HDO of bio-oil model compounds over unsupported sulfided catalysts

Conventional transition metal sulfides (TMS) are typically the molybdenum disulfide supported on a high surface area catalyst support and promoted by Ni or Co as described in Section 2.3. Over recent decades, these traditional TMS catalysts have been tested by omitting the use of catalyst support, resulting in unsupported TMS. Table 3 presents the state-of-the-art of unsupported TMS for phenolic HDO. There are several methods to prepare unsupported TMS, that can be used in the hydrotreatment processes. One of these is a hydrothermal synthesis with synthesis parameters, such as moderate synthesis temperature (150-250 °C) and the absence of hydrogen pressure[43–48]. Wu et al. have prepared a series of hydrophobic unsupported MoS_2, NiS_2-MoS_2, and CoS_2-MoS_2 using hydrothermal synthesis with the aid of silicomolybdic acid for the HDO of 4-ethylphenol[47]. The CoS_2-MoS_2 catalyst achieved a 99.9% 4-ethylphenol conversion with a 99.6% ethylbenzene selectivity after 3 h. The catalyst showed good recyclability after 3 runs at 225 °C[47]. Another study by Wang et al. has proposed a reaction network for p-cresol HDO using a hydrothermally prepared CoMoS catalyst, as shown in Figure 7[43]. Two different deoxygenation routes for p-cresol have been proposed: the first is the DDO route, where the partially hydrogenated dihydrocresol is attacked by the dissociated H^+ and the OH_2^+ species is cleaved in the form of H_2O producing toluene[43]. The second route involves HYD where the partially hydrogenated p-cresol is fully hydrogenated to 4-methylcyclohexanol and then dehydrated to 3-methycyclohexene. The product, 3-methylcyclohexene then underwent hydrogenation and formed methylcyclohexane[43]. The study also described a p-cresol adsorption scheme on an unsupported CoMoS catalyst[43], as shown in Figure 8. P-cresol could adsorb via its vertical orientation and coplanar position in relation to the DDO and HYD routes, respectively[43].

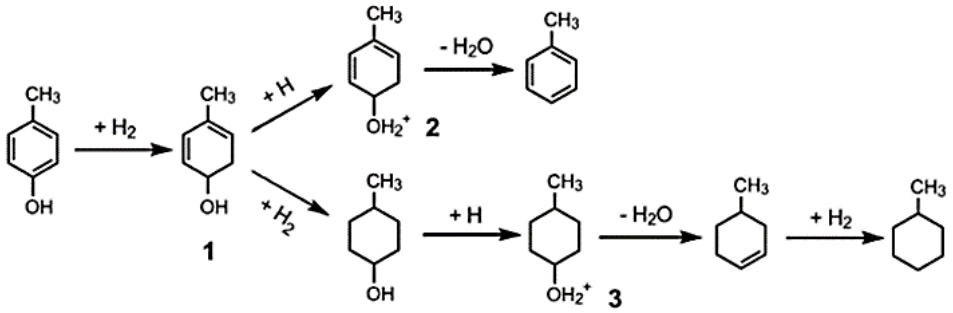

Figure 7. A reaction network for p-cresol HDO over unsupported CoMoS catalyst[43]. Reprinted (adapted) with permission from Wang. W, Zhang. K, Li. L, Wu. K, Liu. P, Yang. Y., *Ind. Eng. Chem. Res.*, 2014, 53 (49), 19001-19009. Copyright (2014) American Chemical Society.

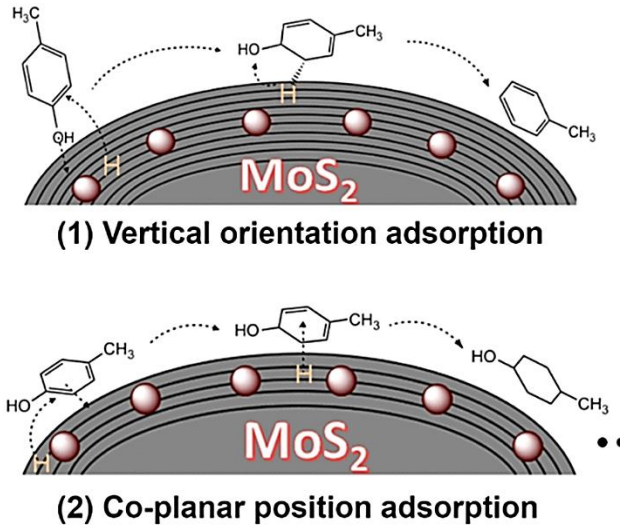

Figure 8. Adsorption scheme for HDO of p-cresol over unsupported CoMoS catalyst[43]. Reprinted (adapted) with permission from Wang. W, Zhang. K, Li. L, Wu. K, Liu. P, Yang. Y., *Ind. Eng. Chem. Res*., 2014, 53 (49), 19001-19009. Copyright (2014) American Chemical Society.

A hard template like mesoporous silica SBA-16 has also been used to synthesize an unsupported NiMoW sulfide catalyst for the HDO of guaiacol in a fixed-bed reactor[49]. The NiMoW sulfide unsupported catalyst gave a 99.6% guaiacol conversion with a minimum coke formation at 400 °C[49]. Adapted from the reference, shown in Figure 9, guaiacol underwent HDO via demethylation (DME), demethoxylation (DMO), and transalkylation[49]. Phenol was formed by either the direct demethoxylation of guaiacol or the dehydroxylation of catechol; both reactions resulted in the production of benzene[49]. It is worth noting that phenol was first obtained from the HDO of guaiacol as a reaction intermediate caused by the higher bond dissociation energy for the hydroxy group in the aromatic ring than in the methoxy group[6].

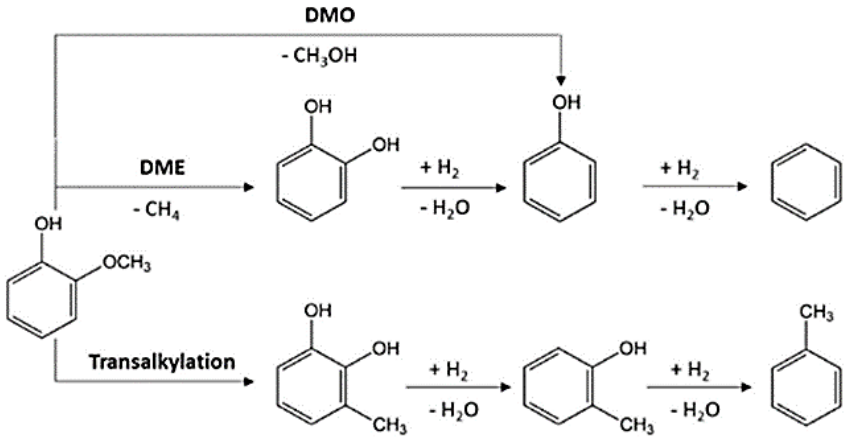

Figure 9. A proposed reaction scheme for HDO of guaiacol over NiMoW catalyst[49]. This article was published in Catalysis Communications, Tran, C. C, Stankovikj, F, Kaliaguine, S, Unsupported Transition Metal-Catalyzed Hydrodeoxygenation of Guaiacol, *Catal. Commun*., 2017, 101, 71–76, Copyright Elsevier (2017).

Table 3. State of the art of sulfided unsupported catalysts for HDO of phenolic oxygenates.

Entry	Sulfided catalyst	Model compound	Solvent	Conversion (%)	Reaction conditions	HDO product selectivity (%)	Ref.
1	MoS_2, NiS_2-MoS_2, and CoS_2-MoS_2	4-ethylphenol and 4-propylguaiacol	Dodecane	44-81.5	Batch, 300 °C, 40 bar, 5 h and 900 rpm	See ref[47]	[47]
2	CoMoS nanosulfide	p-cresol, anisole, and diphenyl ether	Decalin	100 after 3 h (p-cresol)	Batch, 300 °C, 40 bar, and 4 h	Arene yield (98%)	[50]
3	CoS_2/MoS_2	Creosol and phenol derivatives	Dodecane	18-98	Batch, 250 °C, 40 bar, and 1 h	For CoMo-0.3, toluene (99%)	[51]
4	MoS_2 and $CoMoS_2$	Phenol	n-decane	30-98	Batch, 350 °C, 28 bar, 150 rpm, and 1 h	See ref[52]	[52]
5	Amorphous NiMoS	Phenol	n-decane	34.5-96.2	Batch, 350 °C, 28 bar, 150 rpm, and 1 h	For NiMoS-0.3, benzene (30.4%), cyclohexane (52.4%), cyclohexene (9.8%), cyclohexanone (7.4%)	[53]
6	MoS_2	Phenol, 4-methylphenol, and 4-methoxyphenol	Hexadecane	34-52	Batch, 350 °C, 28 bar, 1000 rpm, and 7 h	For phenol, benzene (36%), methylcylohexane (6%) and cyclohexylbenzene (43%)	[54]
7	NiMoW	Guaiacol	-	99	Continuous, 400 °C, 28 bar, and WHSV = 2.7 h^{-1}	Phenol (45%), creosol (15%), catechol (10%), and hydrocarbon (30%)	[49]
8	CoMoS	p-cresol	Dodecane	78.8-98.7	Batch, 350 °C, 28 bar, 900 rpm, and 7 h	For CoMo-0.5-200, methylcyclohexane (6.3%), methylcyclohexene (1.5%) and toluene (92.2%)	[43]
9	Ni-WMoS	p-cresol	Dodecane	85-97.9	Batch, 300 °C, 40 bar, 700 rpm, and 6 h	For W-Mo-0.5, methylcyclohexane (66.7%), methylcyclohexene (3.2%) and toluene (30.3%)	[55]
10	NiMo(W)S	4-methylphenol	Decalin	93.9-97.8	Batch, 300 °C, 30 bar, 800 rpm, and 5 h	Toluene (87.2%), methylcyclohexane (11.3%), and 4-methylcyclohexene (1.5%)	[56]
11	NiMoWS	4-methylphenol	Decalin	87-100	Batch, 300 °C, 30 bar, 800 rpm, and 5 h	Toluene (95.6%), methylcyclohexane (2.9%), and 4-methylcyclohexene (1.5%)	[57]
12	MoP, MoS_2, and MoO_x	4-methylphenol	Decalin	30-100	Batch, 300 °C, 30 bar, 800 rpm, and 5 h	See ref[58]	[58]
13	MoS_2 (effect of adding CTAB)	p-cresol	Dodecane	42-100	Batch, 275 or 300 °C, 40 bar, 900 rpm, and 5 h	See ref[59]	[59]
14	NiMoS	p-cresol	Dodecane	67-100	Batch, 300 °C, 40 bar, 900 rpm, and 5 h	For NiMo-0.3, methylcyclohexane (67.1%), 3-methylcyclohexene (4.12%), and toluene (28.8%)	[60]
15	Fe-MoS_2	p-cresol	Dodecane	63.3-98.3	Batch, 250 °C, 40 bar, 900 rpm, and 5 h	For FeMo-0.3, methylcyclohexane (3.7%), methylcyclohexene (1.6%), and toluene (94.7%)	[61]

2.5 Hydrotreatment of real bio-oils and lignin over sulfided catalysts

The use of model compounds for an HDO reaction cannot fully represent the reactivity of biomass feedstocks. However, the use of model compounds allows quicker evaluation of a catalyst and the elucidation of reaction networks before examining the complex feedstock. This section presents a brief review of studies of the hydrotreatment of biomass feedstocks and lignin over sulfided catalysts, as summarized in Table 4.

In contrast to the pyrolysis or gasification of solid biomass as described in Section 2.1, the one-pot hydrotreatment of lignin or biomass involves the simultaneous depolymerization of the complex structure of lignin into various oxygenated oligomers and fragments which then subsequently undergo full or partial deoxygenation reactions to yield deoxygenated aromatic and alkylphenolic monomers as illustrated in Figure 10. Besides, the depolymerized fragments from lignin may also repolymerize and form char. The undesired char byproducts are usually caused by the saturation and repolymerization of the free radicals formed during the cracking, hydrocracking, and condensation reactions. This one-step process is usually performed in the presence of a solvent under high hydrogen pressure and also high operating temperature. Joffres et. al studied the use of hydrogen donor solvents in the one-step hydrotreatment of wheat straw soda lignin over $NiMoS/Al_2O_3$[62]. Their study highlighted that the use of hydrogen donor solvent such as tetralin is effective in depolymerizing lignin and also limit condensation reactions[62]. The low char production in their experiments can be explained by the stabilization of the free radicals resulting from the cleavage of the C-C or C-H bond during lignin depolymerization with the hydrogen radicals from tetralin[62]. Moreover, in a recent review by Stummann et. al, they highlighted that using a highly active catalyst regardless of the promoter types and support acidity, can suppress the char formation reactions resulting in lesser solid yield[63]. A solvolytic oil from liquified lignocellulosic biomass has been hydrotreated in a batch reactor setup with different hydrogen donor solvents over a series of catalysts such as $NiMo/Al_2O_3$ catalysts in an oxide, reduced, and sulfided form and reduced Pd/Al_2O_3 or carbon[64]. The sulfided NiMo on alumina was found to give excellent liquid product yield with good rheological properties and gross calorific value[64]. Levec et. al., have studied the same liquified solvolysis oil hydrotreated using unsupported MoS_2, Mo_2C, MoO_2, and WS_2 catalysts[65]. They have reported the synthesis of urchin-like MoS_2 interconnected with carbon materials through the sulfidation of Mo precursors, such as MoI_3 and cyclopentadiene-$MoCI_4$[65]. Their work has demonstrated that the synthesized unsupported MoS_2 gives a high selectivity for deoxygenation and possesses a three-times higher dehydroxylation rate than the commercially available bulk MoS_2[65].

Organosolv poplar lignin-derived oil has been subjected to depolymerization using MoS_2 on activated carbon (AC), which resulted in high selectivity for alkylphenols (76.2%)[66]. The study highlights MoS_2/AC as an effective catalyst in simultaneous depolymerization coupled with the demethoxylation of lignin fragments, which produces alkylphenols[66]. Another study has reported Kraft lignin hydrotreatment for the production of alkylphenols using a variety of sulfided Mo and W on various supports promoted by Ni and Co[67]. Sulfided NiW/AC has been found to efficiently depolymerize lignin and yielded 28 wt% of monomers. It also yielded 76% of alkylphenolics and guaiacolics in the course of an 8 h hydrotreatment[67]. The study highlights a few points about lignin depolymerization, and any additional upgrading, and concludes the following items: (i) sulfided catalysts were more active than the oxide catalysts, (ii) W metal was preferred than Mo, (iii) Ni is a better promoter than Co, and (iv) support plays an important role in achieving high product yields, and acidic supports promote char formation. Mukundan et. al. have studied the cleaving of C-C and C-O bonds in lignin using various model compounds and

Kraft lignin over NiMoS on carbon[11]. The catalysts demonstrated good activity in lignin depolymerization, resulting in low molecular compounds comprised of monomers and dimeric aromatics[11]. The excellent catalytic activity was mainly attributed to the absence of support metal interaction, which promotes the formation of the NiMoS phase for deoxygenation activity[11].

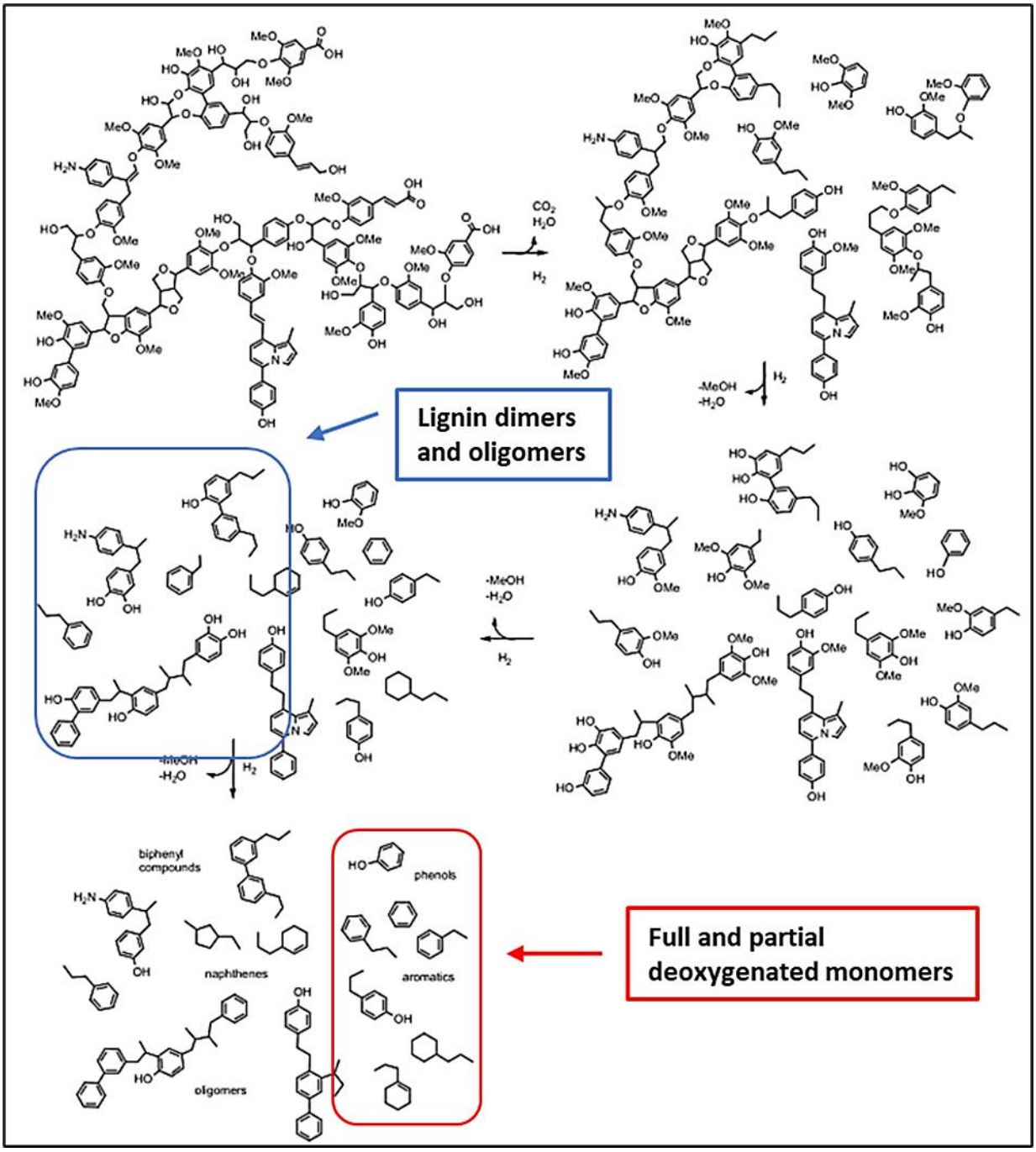

Figure 10. Reaction scheme of lignin hydroconversion over sulfided $NiMo/Al_2O_3$ adapted from reference[62]. This article was published in Applied Catalysis B: Environmental, B. Joffres, M. T. Nguyen, D. Laurenti, C. Lorentz, V. Souchon, N. Charon, A. Daudin, A. Quignard, and C. Geantet., Lignin Hydroconversion on MoS_2-based supported Catalyst: Comprehensive Analysis of Products and Reaction Scheme, *Appl. Catal. B Environ*., 2016, 184, 153–162, Copyright Elsevier (2016).

Table 4. Hydrotreatment of biomass feedstocks over sulfided catalysts.

Entry	Sulfided catalyst	Feedstocks	Solvent	Conversion (%)	Reaction conditions	HDO product selectivity (%) and remarks	Ref.
1	Supported oxide, reduced and sulfided NiMo, Ni, Mo, and Pd	Solvolyzed lignocellulosic biomass	Hydrogen donor solvents (Tetralin, 2-propanol, phenol, m-cresol, anthracene, cyclohexanol, xylene, and pyridine)	-	Semi-continuous, 300 °C, 80 bar, and 1 h	See ref[64]	[64]
2	Unsupported MoS_2, MoO_2, Mo_2C, and WS_2	Solvolyzed lignocellulosic biomass	Tetralin	-	Semi-continuous, 300 °C, 80 bar, and 1 h	See ref[65]	[65]
3	Supported MoS_2	Organosolv poplar lignin oil	Methylcyclohexane	-	Batch, 300 °C, 30 bar, and 10 h	Alkylphenol (76.2%), cycloalkanes (15.5%) and arenes (8.3%)	[66]
4	Supported NiW and NiMo	Kraft lignin	Supercritical methanol	-	Batch, 320 °C, 35 bar, and 8 h	See ref[68]	[68]
5	Supported NiMo and CoMo	Kraft lignin	Solvent-free	65-91	Batch, 350 °C, 100 bar, 1200 rpm, and 4 h	See ref[67]	[67]
6	CoMoS on alumina	Wheat straw soda lignin	Tetralin	91	Semi-continuous, 350 °C, 80 bar, 800 rpm, and 13 h	See ref[69,70]	[69,70]
7	$NiMoS_2$ on carbon	Lignin model compounds and Kraft lignin	Dodecane	-	Batch, 300 °C, 50 bar, catalyst:feed ratio = 1:10, and 3 h	For Kraft ligin experiment, total monomer yield (18.98%)	[11]
8	Commercial sulfided NiMo	Wheat/barley straw bio-oil	-	-	Continuous, 340 °C, 40 bar, feed flow rate $g.h^{-1}$, and TOS of 80 h	See ref[71]	[71]
9	$NiMoS/Al_2O_3$	Wheat straw soda lignin	Tetralin/Dodecane	71-35	Batch, 350 °C, 80 bar, 800 rpm, and 1/14/28 h	See ref[62]	[62]

3 Experimental

This chapter of the thesis describes the catalysts synthesis methods for both studies (Papers I and II), catalyst characterization methods, catalytic test measurements, and product analysis.

3.1 Catalyst synthesis

3.1.1 Supported sulfided catalysts

Unpromoted Mo supported on γ-alumina was prepared using a conventional wet impregnation method following the procedure reported earlier by our group[72]. This unpromoted Mo γ-alumina-supported catalyst was then further loaded with a second transition metal, such as Nickel (Ni), Zinc (Zn), Iron (Fe), or Copper (Cu), via a conventional incipient wetness impregnation method. For instance, a solution of 3 wt.% of $Ni(C_5H_7O_2)_2$ in 20 mL of ethanol was first prepared for the Ni-promoted catalyst. The unpromoted Mo supported on γ-alumina catalyst was dissolved in 25 mL of ethanol. The nickel precursor solution was added dropwise to the solution of the Mo catalyst prepared in the previous step. 10 mL of ethanol was used to wash off the residue in the beaker containing the Ni precursor solution to ensure that all solutions had been transferred. The catalyst slurry was then stirred overnight under a fume-hood to evaporate all the ethanol. The dry catalyst was calcined at 400 °C for 4 h in air. The same procedure was followed for the preparation of FeMo, ZnMo, and CuMo on γ-alumina. Iron (III) acetylacetonate (99%), $Fe(C_5H_7O_2)_3$, Zinc acetylacetonate hydrate (99.995%), and copper (II) nitrate hemi pentahydrate (98%) were used as Fe, Zn, and Cu precursors, respectively. These catalysts were sulfided before the catalytic test and will from this point on be denoted as the Mo, NiMo, ZnMo, FeMo, and CuMo catalysts.

3.1.2 Unsupported sulfided catalysts

A facile hydrothermal synthesis inspired by various studies was followed in the second study to prepare an unsupported MoS_2[73,46]. The preparation steps were modified taking into account the different apparatus available in our laboratory. 0.35 g of ammonium heptamolybdate tetrahydrate (>99%) and 1.3 g of thiourea (>99%) were both first dissolved in 55 mL of distilled water with gentle stirring. The pH of the solution was then adjusted to 0.8 using hydrochloric acid (35 wt.%). This pH alteration step was omitted for one catalyst sample to evaluate the influence of pH adjustment on catalyst properties. After the pH adjustment, the mixed solution was divided equally and transferred to a 70 mL Teflon liner. The filled Teflon liner was then placed and sealed in a stainless-steel autoclave. The mixed solution was heated to 200 ˚C in an oven for either 12 h or 24 h; it took 20 minutes for the oven to reach the desired temperature. After 12 h or 24 h of heating, the oven was cooled to room temperature, and the as-synthesized catalyst (black in color) was collected by filtering and washing the resulting solution in the Teflon liner several times with absolute ethanol. The filtered and washed catalyst was covered and dried under vacuum at 50 ˚C overnight. After vacuum drying, the freshly prepared as-synthesized catalysts were tested in the model reaction without any further treatment. These as-synthesized catalysts were denoted as MoS_2-12 and MoS_2-24, corresponding to the synthesis time. For a second set of samples, the as-synthesized catalysts underwent an annealing pre-treatment at 400 ˚C for 2 h under nitrogen flow prior to their implementation in the model reaction. These pretreated catalysts were then denoted as MoS_2-12a or MoS_2-24a. Commercially available bulk MoS_2 from Sigma-Aldrich in powdered form with a particle size of ~6 µm (max. 40 µm) and a sulfided Mo-supported catalyst were also used in the second study for comparison.

3.2 Kinetics measurements

The HDO kinetics measurement experiments were carried out in a 300 mL stainless steel batch reactor (Parr instruments). The reactor was equipped with a magnetically driven internal stirrer, an inlet that was connected to an H_2/N_2 gas line, an outlet for gas release, and a sampling line for reaction sample collection (0.5 – 2 mL). The reactor set-up is shown in Figure 11.

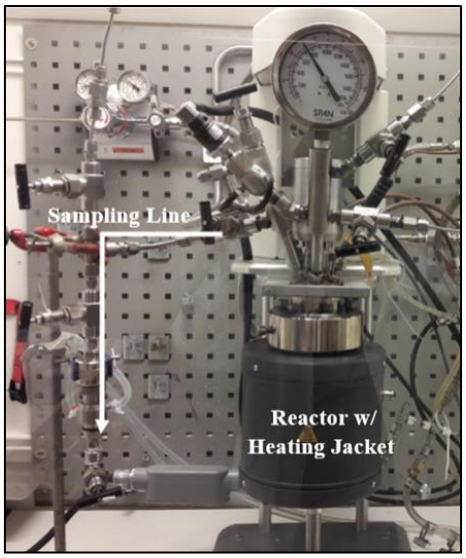

Figure 11. The batch reactor set-up.

Prior to the activity test, 0.5 g of catalyst was sulfided in the batch reactor using 0.5 mL of dimethyl disulfide (≥99.5%, Sigma-Aldrich) with 20 bar of H_2 at 340 °C for 4 h. The reactor was loaded with 1 g of reactant, 0.5 g of pre-sulfided catalyst, 0.1 mL of DMDS, and 100 mL of dodecane for a typical experiment. After loading the reactor with all the reactants, the reactor was first flushed with N_2 three times to remove air, followed by three flushings at 5 bar of H_2. The final reaction conditions for all experiments were set at 300 °C, 50 bar H_2 pressure, and 1000 rpm. Reaction samples were collected at 0.5 h, 1 h, 2 h, 3 h, 4 h, and 5 h. The sampling line was purged with N_2 before collecting the reaction sample. After each reaction sample collection, a small drop in pressure of approx.. 1 bar was observed. The pressure drop was immediately compensated by repressurizing the reactor to maintain the same pressure. When the reaction was finished, the reactor was rapidly cooled to room temperature with a water bath. The spent catalyst was recovered, filtered, centrifuged, and washed with acetone to remove adhering reactants and products. It was then dried under atmospheric conditions for further analysis. The same procedures were followed in the second study. However, 66 mg of unsupported catalyst was used in these experiments.

Part of the first and second studies involved the hydrotreatment of Kraft lignin (KL). The hydrotreatment reaction was carried out in the same batch reactor described above. Prior to the reaction experiment, the reactor was loaded with 0.75 g of catalyst, 2.25 g of KL (Sigma-Aldrich), and 75 mL of hexadecane as a solvent. The catalyst and lignin mass ratio was maintained at 1:3. The final reaction conditions were 340 °C, a total of 70-76 bar of H_2 depending on the catalyst used, and 1000 rpm. The hydrotreatment reaction was monitored for 5 h once the reaction temperature was reached. The heating period took approx. 40 minutes to reach the desired temperature. No reaction

samples were collected for these experiments. When the reaction was completed, all reaction products in liquid form and solid residues were collected in a glass bottle for product analysis.

3.3 Product analysis

The liquid reaction samples were analyzed with a GC-MS (Agilent 7890-5977A). The GC-MS was equipped with a non-polar HP-5 column (30 m × 250 µm × 0.25 µm), a Flame Ionization Detector (the setpoint was 335 °C), and mass spectroscopy for compound identification via the NIST library. The initial oven temperature was 100 °C for 1 minute and then the temperature was increased to 190 °C at a rate of 10 °C/min. The temperature was increased to 300 °C at a heating ramp of 30 °C/min and was maintained constant for 1.333 minutes.

External calibration curves were obtained for 4-propylguaiacol, propylcyclohexane, 4-propylphenol, propylbenzene, 4-propylresorcinol, 1,2-dimethoxy-4-propenylbenzene, gamma terpene, 4-tertbutylanisole, and 2-methyl-6-propyl phenol using commercial chemicals.

The unit for the concentration of reactant and reaction products is expressed in molar percent (mol%). The following definitions were used in this study:

PG conversion was calculated as

$$C_{PG}(\%) = \frac{C_0 - C_t}{C_0} \times 100 \quad (1)$$

where C_0 is the initial concentration of PG and C_t is the concentration of PG at the reaction time equal to t.

Reaction product yields were calculated as

$$Y_{product}(\%) = \frac{C_{product,t}}{C_0} \times 100 \quad (2)$$

where $C_{product,\,t}$ is the concentration of the reaction product at the reaction time t.

Reaction product selectivities were calculated as

$$S_{product}(\%) = \frac{C_{product,t}}{C_0 - C_t} \times 100 \quad (3)$$

The molar balance was calculated to evaluate the material balance in the liquid phase of the HDO reaction. The molar balance was calculated by dividing the sum of the concentration of all identified reaction products and the initial feed at reaction time t by the concentration of the initial feed at time zero. The carbon balance on the liquid phase was checked for all reported experiments and found to be in the range between 95% and 99%. The missing carbon from the balance calculations could be attributed to the experimental errors and also small amounts of light hydrocarbons and carbon oxide byproducts in the gas phase after the reaction.

The same GC-MS was used in the second study to analyze the bio-liquid products from the catalytic hydrotreatment of KL. The initial GC oven temperature was 50 °C for 5 minutes and then the temperature was increased to 300 °C at a rate of 10 °C/min. This was maintained constant for 5 minutes. The solid residues obtained from the filtration of the bio-liquid were washed first with acetone and then dried in an oven at 80 °C overnight. The unconverted lignin retained in the dried solid was dissolved with dimethyl sulfoxide (DMSO) washing. After dissolving the unconverted lignin with DMSO, the solid product was dried again in the oven at 80 °C overnight.

The bio-liquid products were also in some cases analyzed with 2D GC × GC-MS-FID (Agilent 7890B) gas chromatography equipped with an oven, a flow splitter, a modulator, and a flame ionization detector. The injector temperature was 280 ˚C and the sample injection volume was 1 µL. Helium gas was used as a carrier gas with a flow rate of 1 mL/min with a split ratio of 30. The chromatographic separation involved two columns: a mid-polar phase column VF-1701MS (30 m × 250 µm × 0.25 µm) and a non-polar phase column DB-5MS UI (1.2 m × 150 µm × 0.15 µm). Modulation time on the modulator was 8 s. The oven temperature was initially set at 40 °C for 1 min and then heated up to 280 °C at a rate of 2 °C/min. The flame ionization detector temperature was set at 250 °C. The hydrogen flow rate was 30 mL/min and the airflow rate was 350 mL/min. The analysis was performed using the GCImage software for multidimensional chromatography. The individual product selectivity in the liquid was calculated by dividing the corresponding MS blob volume of the product by the total MS blob volume for all identifiable products in the liquids.

The initial solid residues obtained after filtration should contain spent catalyst, solid char, and unconverted lignin. The weight of the solid was recorded after each drying. Kraft lignin conversion was calculated based on the difference between the initial Kraft lignin feed and the unconverted lignin divided by the initial lignin feed.

Char amount (g) = Total solid residues (g) – 0.75 g of catalyst – unconverted lignin (g)

Char yield (%) = Char amount (g) /2.25 g of initial Kraft lignin feed × 100%

3.4 Catalyst characterizations

3.4.1 Nitrogen (N_2) physisorption

Textural properties, such as specific surface area, pore volume, and the pore size of the catalysts, were measured with N_2 physisorption at -196 °C using a Tristar 3000 gas analyzer. The supported catalysts (approximately 0.3 g) were degassed in a quartz tube at 250 °C for 2 h under N_2 flow to remove moisture, and the unsupported catalysts (approximately 0.15 g) were degassed at 300 °C overnight. The specific surface area and pore sizes of the catalysts were calculated by the Brunauer-Emmett-Teller (BET) method and Barrett-Joyner-Halenda (BJH) method, respectively.

3.4.2 X-ray powder diffraction (XRD)

XRD was used to identify the crystalline phases of the synthesized catalysts in this work. X-ray diffractograms for all catalysts were obtained using an X-ray powder diffractometer operated at 40 kV and 40 mA (Bruker AXSD8 Advance) with a CuKα monochromatic radiation (λ=1.542A°) source in the 2θ range of 10°-80°.

3.4.3 X-ray photoelectron spectroscopy (XPS)

The chemical state and composition of the catalysts were measured with XPS. The measurements were carried out using a Perkin Elmer PHI 5000 VersaProbe III Scanning XPS Microprobe. The monochromatic Al-Kα X-ray source with a binding energy of 1486.6 eV was operated in the analysis chamber. The core-level spectra of Mo 3d, O1s, S2p, and C1s were recorded with a step size of 0.1 eV. The software Casa XPS with the C1s binding energy at 284.8 eV as a reference was used to analyze the raw data with a Shirley background.

3.4.4 Raman spectroscopy

Raman spectra were obtained using a WITec alpha300 R Confocal Raman microscope equipped with a thermoelectrically cooled (-60 °C) EMCCD detector. A 532 nm CW diode laser at 0.3 mW was used for excitation and the light was focused on the sample with a 100X/NA0.9 objective. The Raman scattering was collected using

the same objective and was spectrally resolved using an 1800 groves/nm grating. The position of the Raman spectra bands was calibrated using the silicon peak at 519.3 nm.

3.4.5 Electron microscopy (SEM & TEM)

The morphologies and structure of the catalysts were investigated using scanning and transmission electron microscopy, SEM, and TEM. The SEM images for the unsupported MoS_2 in the second study were acquired using a JEOL 7800F Prime scanning electron microscope. The particle diameter of over two hundred MoS_2 particles from the SEM images was measured with ImageJ software and further calculated to obtain the average particle sizes.

The TEM images for both studies were acquired using an FEI Titan 80-300 transmission electron microscope (TEM) operated at an accelerating voltage of 300 kV. A high-angle annular dark-field (HAADF) was used to acquire scanning TEM (STEM) images. Energy dispersive X-ray (EDX) analysis was performed using an Oxford X-sight detector in STEM mode to identify the chemical elements in the catalyst samples. TEM Imaging & Analysis (TIA) software was used for data analysis and spectrum acquisition. 15-25 representative images were used for data analysis. The ImageJ software was used to measure and process approximately 300-350 MoS_2 slabs.

The following equations were used to calculate the average MoS_2 slab length (ΔL) and stacking number (Δn)[74]:

$$\text{Average } MoS_2 \text{ slab length } (\Delta L) = \frac{\sum_i^n x_i l_i}{\sum_i^n x_i} \quad (4)$$

$$\text{Average stacking number } (\Delta n) = \frac{\sum_i^n x_i N_i}{\sum_i^n x_i} \quad (5)$$

where $\boldsymbol{i}$ is the total number of MoS_2 slabs. $\boldsymbol{x_i}$ is the number of MoS_2 slabs with $\boldsymbol{N_i}$ layers of length $\boldsymbol{l_i}$. $\boldsymbol{N_i}$ is the stacking number, and $\boldsymbol{l_i}$ is the MoS_2 slab length.

We also calculated the MoS_2 dispersion ($\boldsymbol{f_{mo}}$) of the catalysts with the following equation reported in the literature[74]:

$$MoS_2 \text{ dispersion } (\mathbf{f_{mo}}) = \frac{\boldsymbol{Mo_{edge}}}{\boldsymbol{Mo_{total}}} = \frac{\sum_i^m \mathbf{6}(\boldsymbol{n_i}-\mathbf{1})}{\sum_i^m (\mathbf{3}\boldsymbol{n_i}^2-\mathbf{3}\boldsymbol{n_i}+\mathbf{1})} \quad (6)$$

where $\boldsymbol{Mo_{edge}}$ is the number of Mo atoms located on the edges of the MoS_2 slabs, and $\boldsymbol{Mo_{total}}$ is the total number of Mo atoms. $\boldsymbol{n_i}$ is the number of Mo atoms along the edge of the MoS_2 slabs with its length obtained by calculation (L = 3.2(2$\boldsymbol{n_i}$ -1) Å), and $\boldsymbol{m}$ is the total number of MoS_2 slabs obtained from the TEM images of different catalysts.

The edge-to-corner ratio of MoS_2 slabs was calculated based on the following equation[75]:

$$\frac{\boldsymbol{f_{edge}}}{\boldsymbol{f_{corner}}} = \frac{5\Delta L}{3.2} - 1.5 \quad (7)$$

4 Results and discussion

This chapter presents the results and a discussion based on the two independent studies presented in Papers I and II. In the first study (Paper I), the effect of Ni, Fe, Zn, and Cu on a conventional MoS_2 supported on γ-alumina catalyst was studied in a model reaction, the HDO of PG at 300 °C, 50 bar H_2 pressure, and 1000 rpm for 5 h. The PG conversion, reaction product yield, and selectivity for all catalyst systems were examined. The characterization results are reported here to explain the different properties of the catalysts. We proposed a reaction network for the HDO of PG over the sulfided catalysts, and kinetic modeling was performed to validate the experimental data. The influence of the impregnation of the transition metals on the rates of different reactions in the HDO of PG was studied. In the second study (Paper II), the activity and selectivity of the as-synthesized and annealed unsupported MoS_2 catalysts prepared using a hydrothermal method were studied for the HDO of PG. The effect of synthesis parameters, such as synthesis time and pH adjustment, on the unsupported MoS_2 catalyst, were investigated. The activity of an annealed unsupported MoS_2 catalyst in the hydrotreatment of Kraft lignin was demonstrated. A comparison was made between a bulk MoS_2 catalyst in the HDO of PG and the hydrotreatment of Kraft lignin.

4.1 Role of transition metals on MoS_2-based supported catalysts for hydrodeoxygenation (HDO) of Propylguaiacol

4.1.1 HDO of PG over supported Mo sulfided catalysts

The effect of Ni, Fe, Zn, and Cu on γ-alumina-supported MoS_2 was studied using the HDO of PG in a batch reactor. Figure 12 shows the conversion of PG for Mo, NiMo, FeMo, ZnMo, and CuMo sulfided catalysts. Complete PG conversion was obtained after 2-3 hours for all catalysts (Figure 12).

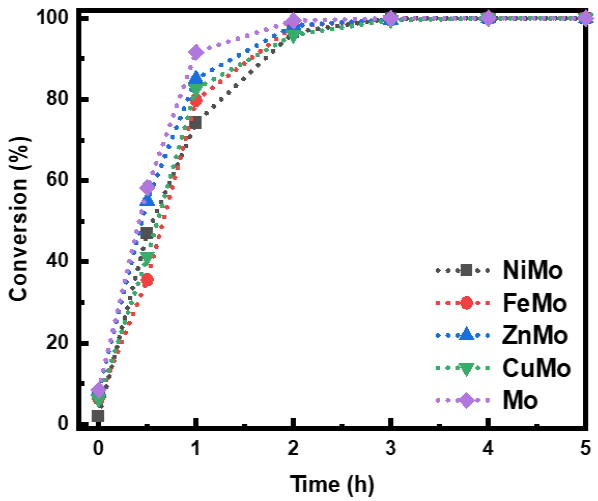

Figure 12. PG conversion (%) versus time (h). Reaction conditions: 300 °C, 50 bar H_2, 1000 rpm, and 5 h reaction.

One hour was the reference time for comparison, and a 91% PG conversion was achieved for the sulfided Mo catalyst, which was the highest conversion of all the catalysts. In contrast, the NiMo sulfided catalyst showed a 74% PG conversion after 1 h. A decrease in the PG conversion after 1 h was observed in the order of Mo > ZnMo > CuMo > FeMo > NiMo. The results show that the bimetallic catalysts had a lower conversion after 1 h; the NiMo had the lowest conversion. The lower conversion for the bimetallic catalysts at the earlier stage of the reaction (1-2 h) can be attributed to the slower rate in the demethoxylation of PG, forming 4-propylphenol as the

first step in the deoxygenation route. Different reactions, such as demethoxylation, dehydroxylation, hydrogenolysis, hydrogenation, transalkylation, and isomerization, occurred at different times during the 5-hour reaction. A pool of products was formed, including partially deoxygenated compounds such as phenolics, deoxygenated aromatics, and cycloalkane compounds. To facilitate the analysis, the reaction products and intermediates were grouped into different classes that included compounds with two oxygen atoms, phenolics, aromatics, and cycloalkanes, as listed in Figure 13.

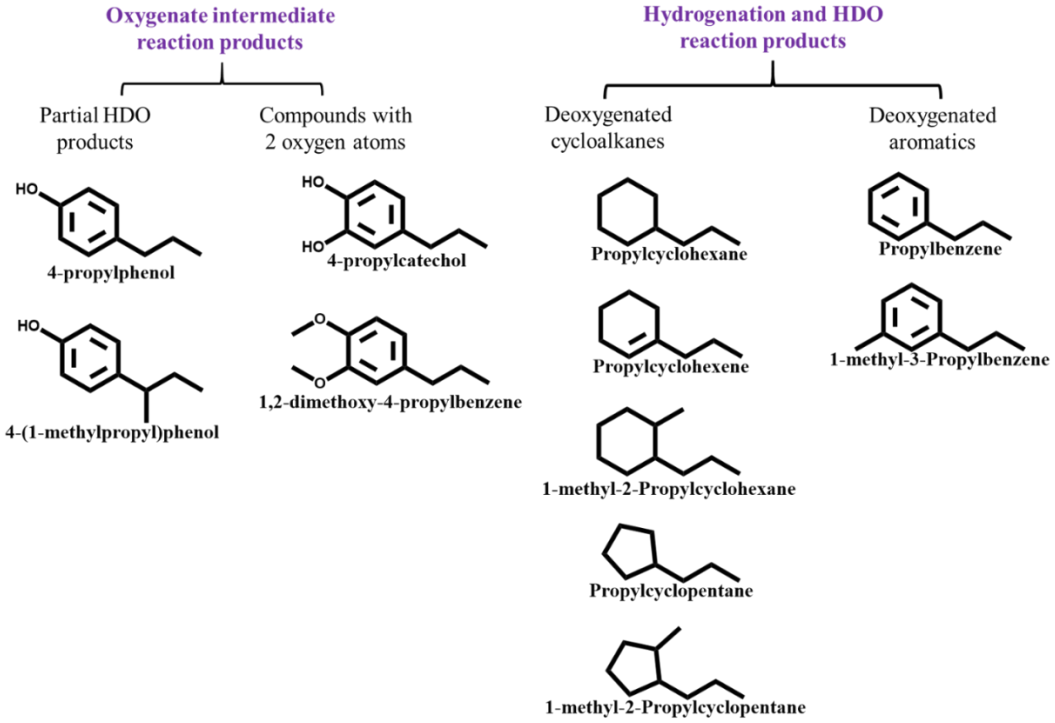

Figure 13. Classes for reaction products and intermediates from HDO of PG: oxygenate intermediates and hydrogenation and HDO reaction products.

The evolution of products and intermediates versus reaction time for the HDO of PG over all the studied catalysts is illustrated in Figure 14. The demethoxylation of PG that formed 4-propylphenol was the first step in the deoxygenation route as the yield of the phenolics (mainly 4-propylphenol) increased to a maximum after 1-2 hours reaction time. The suppression of the yield of phenolics that occurred afterward can be explained by the dehydroxylation of 4-propylphenol, which underwent hydrogenation and produced propylcyclohexane and propylcyclohexene. It has been reported in the literature that intermediates such as 4-propylcyclohexanone, resulting from the keto-enol tautomerization of partially hydrogenated 4-propylphenol, have been found in the HDO of isoeugenol using non-sulfided catalysts[76,77]. However, we did not find 4-propylcyclohexanone when sulfided catalysts were used, indicating that the primary route for the formation of propylcyclohexane was from the dehydroxylation of 4-propylphenol and the further hydrogenation of propylbenzene. This result implies that direct deoxygenation (DDO) is the dominant deoxygenation pathway for HDO of PG over these bimetallic sulfided catalysts which was consistent with the findings from literature studies[31,43]. Trace amounts of two-oxygen-atom compounds, such as 4-propylcatechol and 1,2-dimethoxy-4-propylbenzene, were detected after 30 minutes for all catalysts and were suppressed after 2-3 hours (see Figure 14). 9% of oxygenates were found in the liquid products when using sulfided Mo catalysts, and 19% were found when using NiMo catalysts after 30 minutes.

The yield of deoxygenated cycloalkanes was studied for each catalyst (see Figure 14). The cycloalkanes detected in all the experiments included propylcyclohexane, propylcyclohexene, propylcyclopentane, 1-methyl-2-propylcyclopentane, 1-methyl-2-propylcyclohexane. Propylcyclohexane was the major compound detected in all the catalyst systems. The production of deoxygenated cycloalkanes dominated in the latter part of the reaction for all catalysts, except for the CuMo catalyst. For example, a 70.2% cycloalkane yield was achieved for the Mo catalyst after 5 h, as shown in Figure 14(a). 4.5% of 1-methyl-2-propylcyclopentane was formed after 5 h, which resulted from the ring contraction that occurred during the reaction in addition to deoxygenation and ring hydrogenation. The same cyclopentane-derived compound was obtained for the NiMo, ZnMo, and FeMo catalysts, which gave a final yield of 3%, 4.6%, and 4.5%, respectively. A comparison between the catalysts showed that the sulfided NiMo catalyst gave the highest yield of deoxygenated cycloalkane at 94%. In contrast, the total deoxygenated cycloalkane yield was 58.1%, 67.2%, and 44.4% for FeMo, ZnMo, and CuMo catalysts, respectively. The results show that the sulfided NiMo catalyst was the most efficient at deoxygenation of all catalysts, and the impregnation of Fe, Zn, and Cu slowed the deoxygenation rate; Cu was the most inefficient. The better HDO activity for the NiMo catalyst was attributed to the high dispersion of active particles, as found from the TEM analysis in Section 4.1.2. However, a better MoS_2 dispersion may not be the only deciding factor to achieve better HDO activity when relating the catalytic activity results obtained using ZnMo, FeMo, and CuMo sulfided catalysts in HDO of PG. For instance, the ability of the added metal to interact with Mo and promote the formation of sulfur vacancy sites may be of primary importance[78].

All classes of compounds produced using HDO were considered during the study. It is worth mentioning the importance of the production of aromatic compounds as they can be blended with gasoline to improve the octane number[79]. Aromatic compounds can serve as an important feedstock for bulk chemical production[80]. Figure 14a) shows that the Mo catalyst reached a final yield of aromatic compounds of 12% which contains propylbenzene and 1-methyl-3-propylbenzene. The sulfided FeMo and ZnMo catalysts afforded a final deoxygenated aromatic yield of 16% and 19%, respectively. In contrast, the high aromatic hydrogenation activity for sulfided NiMo catalysts resulted in only 7% of deoxygenated aromatics. The results show that the incorporation of Fe and Zn into the traditional hydrotreating catalyst can suppress the hydrogenation activity of the catalyst, yielding more deoxygenated aromatics. The sulfided Mo catalyst provided a deoxygenated compound yield of 82.1%. The sulfided NiMo catalyst exhibited complete deoxygenation after 5 h. The deoxygenated compounds yield was 86.6%, 74.3%, and 50.1% for sulfided ZnMo, FeMo, and CuMo catalysts, respectively. These findings indicate that the sulfided NiMo catalyst was able to deoxygenate efficiently, while the sulfided ZnMo catalyst was able to improve PG deoxygenation better than the sulfided Mo catalyst. In contrast, the sulfided FeMo and CuMo catalysts repressed the formation of deoxygenated compounds.

The evolution of phenolics was investigated for all catalyst systems. Figure 14b) shows that the yield of phenolics reached a maximum of 34% after 2 h for NiMo catalysts. The Mo catalyst had a maximum yield of 44% of phenolics, as shown in Figure 14a). This result explains the faster demethoxylation rate of PG for the unpromoted catalysts than for the Ni-promoted catalyst. The same result was found for sulfided ZnMo (Figure 14d)), which had a 36% yield after 1 h. CuMo sulfided catalysts had a steady increase in phenolic yield to 53.8% in 3 h (Figure 14c)), but the final yield was 47%. The sulfided FeMo catalyst (Figure 14e)) had a maximum of 54% phenolic yield after 2 h, and this decreased to 26% at the end of the reaction. The sulfided CuMo catalyst had the highest phenolic yield, implying that it had the lowest deoxygenation activity of all the sulfided catalysts.

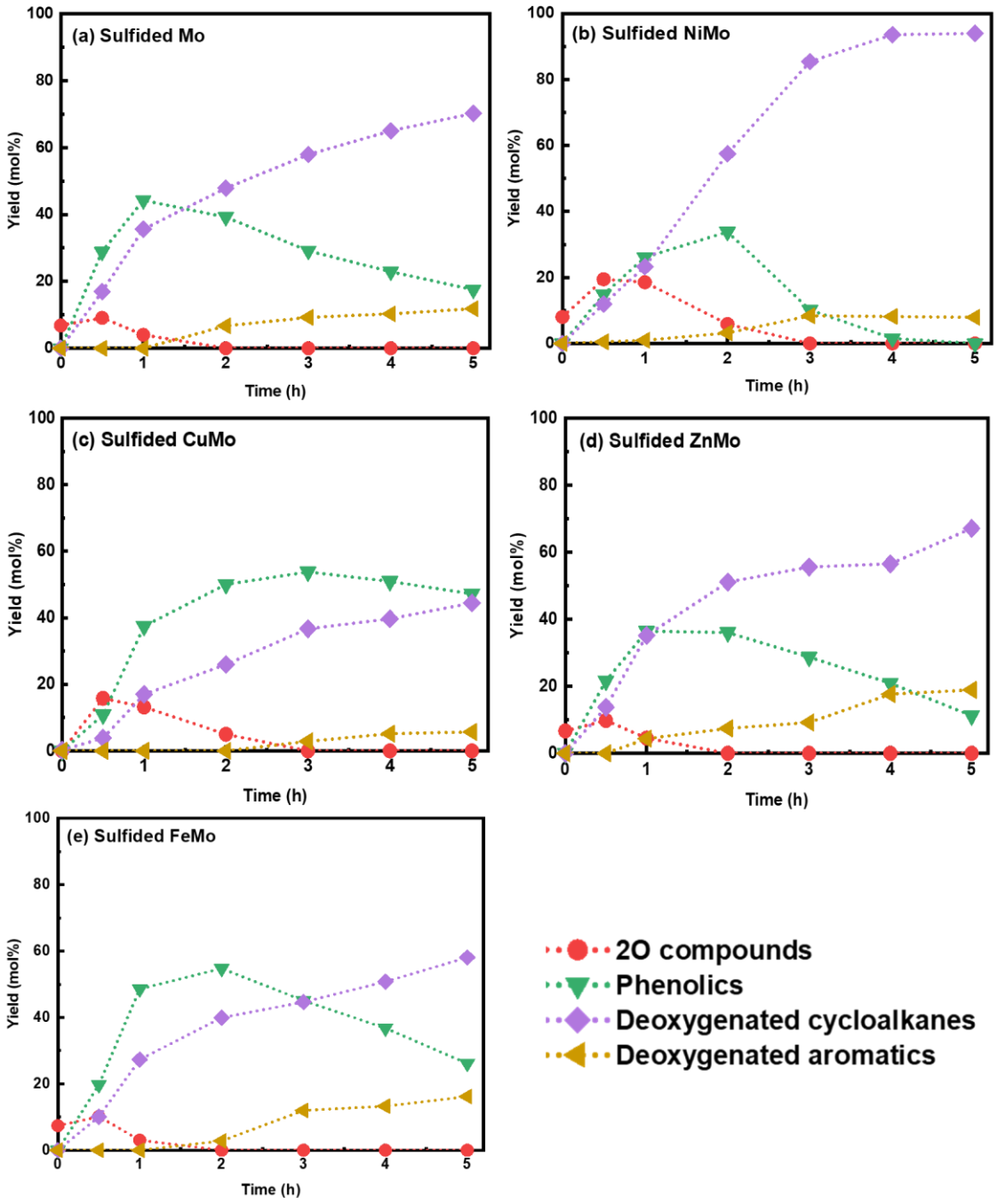

Figure 14. Reaction product evolution for HDO of PG over (a) Mo, (b) NiMo, (d) ZnMo, and (e) FeMo catalysts. Reaction conditions: 300 °C, 50 bar H_2, 1000 rpm, and 5 h reaction. Markers present the experimental points.

4.1.2 Catalyst characterization

The metal loadings and textural properties of the as-synthesized catalysts were verified with ICP-MS and N_2 physisorption, as shown in Table 5. The specific surface area and pore volume of the catalysts were reduced after the metal impregnation, indicating pore blockage.

Table 5. Elemental composition (wt%) and N_2 physisorption results for the as-synthesized catalysts.

Catalyst	Elemental composition, (wt%)					N_2 physisorption		
	Mo	Ni	Cu	Fe	Zn	S_a*	V_p*	d_p*
Mo	13.2	-	-	-	-	155	0.36	93.2
NiMo	13.4	3.47	-	-	-	133	0.29	87.2
CuMo	12.4	-	3.32	-	-	144	0.32	89.2
FeMo	12.3	-	-	2.47	-	139	0.34	97.7
ZnMo	11.0	-	-	-	2.23	141	0.34	96.3

*S_a = BET surface area (m^2g^{-1}), V_p = Pore volume (cm^3g^{-1}), d_p = Average pore size (Å)

The XRD patterns in Figure 15 represent the freshly sulfided catalysts and γ-alumina. All diffraction peaks corresponding to γ-alumina were visible in all catalysts[81]. In contrast, there were no diffraction peaks related to MoS_2, indicating a well-dispersed MoS_2 phase on the support and lower crystallinity for the supported catalysts. Metal sulfided phases, such as NiS, FeS, FeS_2, and CuS, were not identified in the diffractograms, which could mainly be attributed to the low metal loading of the catalysts. Interestingly, the sulfided ZnMo catalyst had three characteristics peaks at 2θ = 28.6°, 47.6°, and 56.5°, corresponding to (111), (220), and (311) planes, showing the presence of the ZnS phases[82].

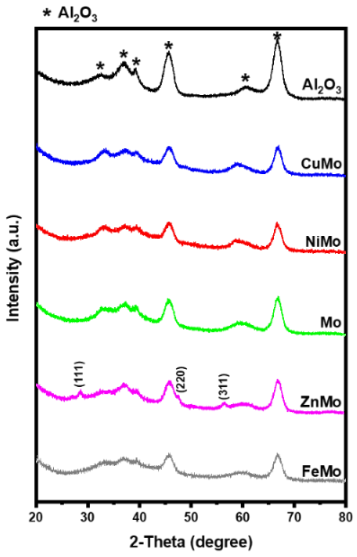

Figure 15. XRD analysis for all sulfided catalysts and alumina.

XPS measurements were performed to understand the chemical and electronic state of the sulfided catalysts. All representative spectra for the sulfided catalysts are shown in Supporting Information in Paper I. Table 6 shows the Mo degree of sulfidation for all sulfided catalysts. This was calculated based on the contribution of Mo^{4+} over the total Mo species (Mo^{4+}, Mo^{5+}, and Mo^{6+}) determined from the Mo 3d core-level spectrum. The presence of Mo^{5+} and Mo^{6+} was attributed to the surface re-oxidized MoS_2 during the analysis and the incomplete sulfidation of the

catalysts. Ni species, such as Ni^{2+}, NiMoS, and NiS_x, were visible in the Ni 2p spectrum of the sulfided NiMo catalyst[83]. Cu^{+} species and pure Cu metal were visible in the Cu 2p spectrum of the sulfided CuMo catalyst[84]. The Fe 2p spectrum also had binding energies of Fe^{2+} and Fe^{3+}, indicating the presence of both species[61]. Characteristic peaks corresponding to Zn^{2+} species were visible, corroborating the results from XRD and showing the presence of ZnS.

Table 6. Mo 3d XPS results for supported sulfided catalysts

Catalyst	$Mo_{sulfidation}$ (%)	Binding energy (eV)					
		Mo^{4+}		Mo^{5+}		Mo^{6+}	
		$3d_{5/2}$	$3d_{3/2}$	$3d_{5/2}$	$3d_{3/2}$	$3d_{5/2}$	$3d_{3/2}$
Mo	69.2	228.7	231.8	-	-	232.4	235.5
NiMo	57.9	229.3	232.4	-	-	232.5	235.6
CuMo	28.4	229.3	232.4	230.6	233.7	233.7	236.9
FeMo	92.3	229.1	232.5	-	-	233.7	236.1
ZnMo	83.1	228.9	232.1	-	-	233.7	235.6

The morphologies of all sulfided catalysts were examined with TEM, as shown in Figure 16. Typical linear and curvy MoS_2 black fringes scattered around were visible in all TEM images, as shown in Figure 16(a-e). The interplanar distance of 0.64 nm corresponding to the characteristic basal plane of MoS_2 can be seen in the TEM images. Table 7 presents the statistical results for the average slab length and average stacking layer for MoS_2, MoS_2 dispersion, and the edge-to-corner ratio for a MoS_2 slab. The distributions for the number of MoS_2 stack layers and slab lengths are shown in Figure 17. The number of stacks in all the catalysts was in the range from one to six; one was the most frequent. Slab lengths were mostly between 4 nm and 6 nm. It is clear that the doping of different metals on the Mo catalyst reduced the slab length and increased the stacking layer of MoS_2, as shown in Table 7. This could result from the metal species hindering the growth of MoS_2 fringes during sulfidation. Overall, the increase in the average stacking layer of the metal-doped catalysts and the reduction in slab lengths improved the dispersion of MoS_2. The better dispersion of MoS_2 was also confirmed by the absence of MoS_2 peaks in the XRD analysis. Improvement in MoS_2 dispersion also increased the exposure of active edges to the catalytic reaction. Elemental mapping was performed on a selected area at the edge of the NiMo catalysts, as shown in Figure 16(f), and the results indicate that there was an even distribution of Ni, Mo, and S elements on the catalyst surface. The better dispersion of the active particles for NiMo catalyst as compared to the base Mo catalyst may contribute to improved HDO activities, as demonstrated by the NiMo catalyst in Section 4.1.1.

Table 7. TEM analysis of sulfided catalysts.

Sulfided Catalysts	Average slab length (ΔL), nm	Average stacking degree (Δn)	MoS_2 Dispersion (f_{Mo})	Mo edge-to-corner ratio $(f_{edge}/f_{corner})_{Mo}$
Mo	5.643	1.952	0.139	7.317
NiMo	5.099	2.162	0.146	6.467
CuMo	5.018	1.958	0.153	6.341
FeMo	5.145	1.870	0.149	6.539
ZnMo	4.232	2.074	0.168	5.113

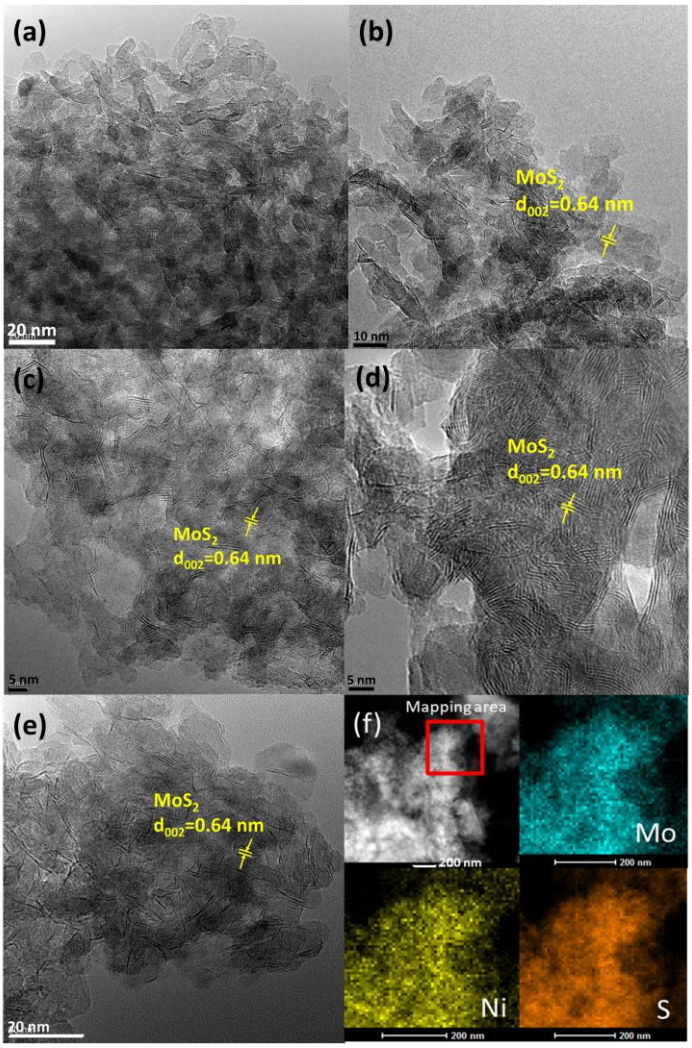

Figure 16. TEM images of (a) Mo, (b) NiMo (c) CuMo, (d) ZnMo, (e) FeMo sulfided catalysts, and (f) HAADF STEM-EDX images of NiMo sulfided catalyst.

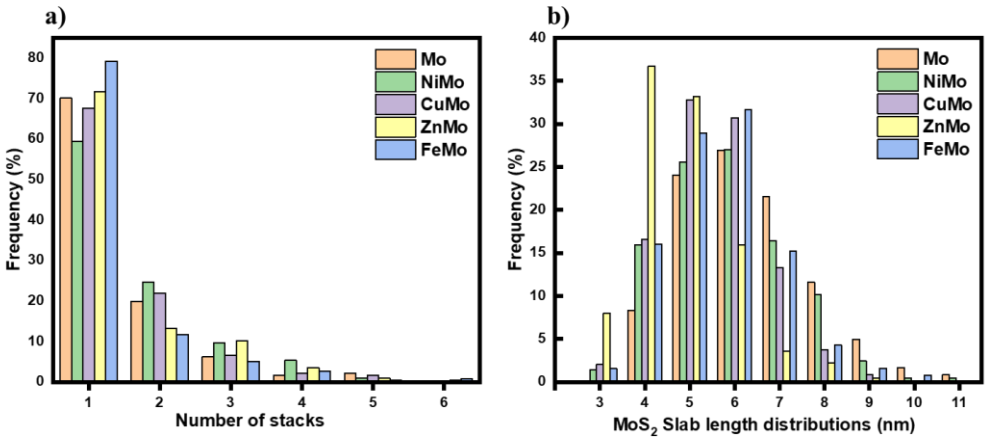

Figure 17. The (a) number of stacks and (b) distribution of MoS_2 slab lengths for all sulfided catalysts.

4.1.3 Modeling the reaction network for HDO of PG over sulfided catalysts

A reaction network for the HDO of PG over different sulfided catalysts was proposed, as shown in Scheme 3 based on the kinetics results and research articles on phenolics HDO. Under the studied reaction parameters, PG underwent demethoxylation, producing 4-propylphenol as a major intermediate that was seen in all the catalytic reactions. A trace amount of two-oxygen-containing compounds, such as 4-propylcatechol and 1,2-dimethoxyl-4-propylbenzene, were also visible at the onset of the reaction, but when the reaction had progressed, the corresponding yield of these compounds decreased. Since the concentration of these compounds was low at the beginning of the reaction, they were lumped together as a sum to study the evolution of such products. The production of dimethoxyl-4-propylbenzene can be explained by the intermolecular transfer of the methyl group to the hydroxyl group[85,86]. 4-propylphenol was then further converted to propylbenzene through hydrogenolysis and deoxygenation reactions. Deoxygenated cycloalkanes, such as propylcyclohexane, were formed through the hydrogenation of propylbenzene. A partially hydrogenated compound like propylcyclohexene was also observed during the reaction. Some alkylated products, such as 4-(1-methylpropyl)phenol and 1-methyl-3-propylbenzene, were detected in low concentrations during the reaction[87]. Different reaction products detected during the 5 h reaction were grouped into phenolics, partial HDO products, deoxygenated cycloalkanes, and aromatics, as shown in Figure 13.

One of the objectives of this study was to understand the reaction network of bio-oil model compounds when sulfided catalysts are used. Another objective was to study how the doping of different transition metals into conventional hydrotreating catalysts can affect the rates of different reactions that take place during the HDO of PG. Hence, a simple modeling study of the HDO of PG was performed based on the kinetic results obtained in the experimental work. Several studies have reported the kinetics for phenolics HDO using zirconia-supported Rh catalysts[88], Pt- and Ir-modified bifunctional catalysts[89], carbon-supported metal catalysts[90], and sulfated Ni promoted zirconia on SBA-15[77]. Studies on the reaction behaviors of phenolics using sulfided catalysts coupled with modeling are scarce.

A simple pseudo-first-kinetic model was used to fit the experimental data for the PG HDO obtained in the batch setup. The low complexity and the low numbers of parameters to be estimated were the reason for the model selection. The hydrogen concentration and catalyst mass in all experiments were assumed to be constant throughout the reaction and were lumped together in the apparent rate constants, as listed below in the rate equations. All reaction parameters were kept constant for all experiments for comparable kinetic constants.

The development of the kinetic model first involved the construction of a simple model by considering a simplified route as ‘a: 4-propylguaiacol → b: 4-propylphenol → c: propylbenzene → d: propylcyclohexane’ based on the proposed reaction route in Scheme 3. The rate equation corresponding to each reaction was defined as follows:

$$r_1 = k_1 c_a \quad (8)$$

$$r_2 = k_2 c_b \quad (9)$$

$$r_3 = k_3 c_c \quad (10)$$

A set of ordinary differential equations (ODE) for the batch reactor material balance was considered:

$$\frac{dC_a}{dt} = -r_1 \quad (11)$$

$$\frac{dC_b}{dt} = -r_2 + r_1 \quad (12)$$

$$\frac{dC_c}{dt} = -r_3 + r_2 \quad (13)$$

$$\frac{dC_d}{dt} = r_3 \quad (14)$$

These ODEs were then solved numerically with the MATLAB ode15s function. Experimental results for the kinetic model were fitted to estimate the kinetic constant for all involved reactions during the HDO of PG. The residual sum of squares (SSres) was minimized and defined as follows:

$$\text{SSres} = \sum(C_{exp,t} - C_{model,t})^2 \quad (15)$$

where $C_{exp,t}$ is the concentration of different reaction products obtained from experimental values, and $C_{model,t}$ is the estimated concentration from the kinetic model.

The coefficient of determination (R^2) was defined as follows:

$$R^2 = \left(1 - \frac{\sum(C_{exp,t} - C_{model,t})^2}{\sum(C_{exp,t} - C_{mean})^2}\right) \times 100 \quad (16)$$

where C_{mean} is the mean value of the parameter. The coefficient of determination was used as an indication of the feasibility of the kinetic model when applied to all sulfided catalyst systems.

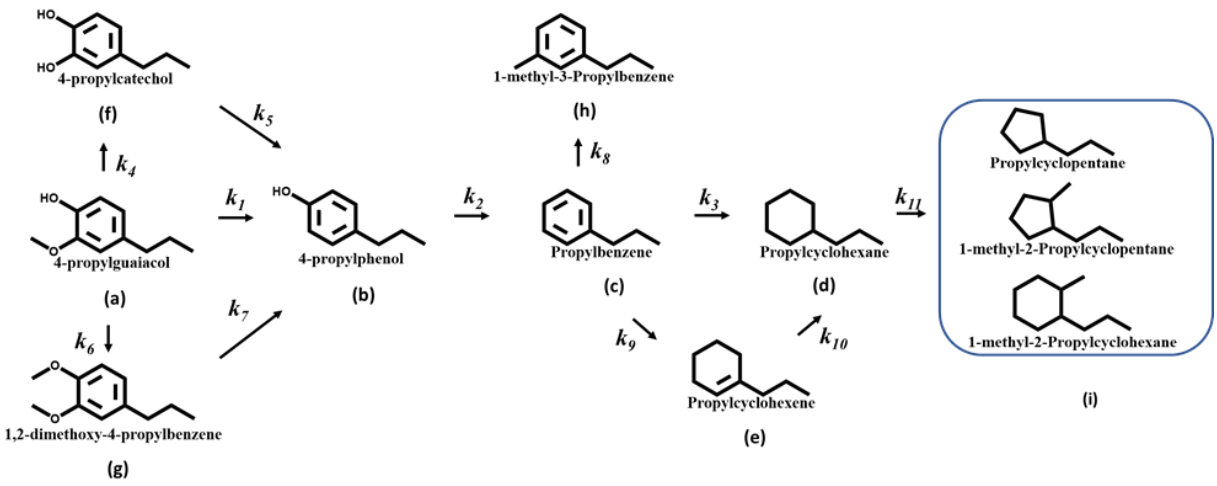

Scheme 3. A proposed reaction network for HDO of PG over different sulfided catalysts.

Figure 18 shows the kinetic fitting results obtained using the simplified kinetic model and illustrates the concentration trend of PG, 4-propylphenol, propylbenzene, and propylcyclohexane. The plot of the simplified kinetic model was able to describe the deoxygenation route of PG. The deoxygenation route for PG first involved the cleaving of the methoxy group and followed by the formation of propylphenol, then there was a further cleaving of the hydroxyl group, which produced propylbenzene. 90.5% of the coefficient of determination was obtained for this simple model, indicating a good description of experimental data. However, the side reactions were omitted from this model, and some clear deviations in the data points can be seen in Figure 18.

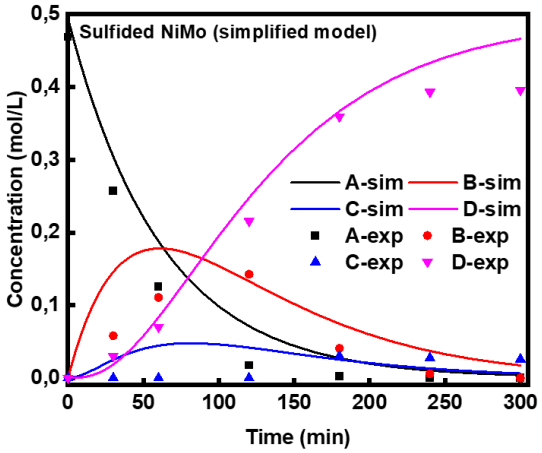

Figure 18. Product concentration profiles for PG HDO over sulfided NiMo catalyst using the simplified model. A: PG, B: 4-propylphenol, C: Propylbenzene, and D: Propylcyclohexane. The solid line represents the modeling results, and the symbol represents the experimental results.

The simplified model was then improved by considering all the side reactions that occurred during the HDO of PG as shown in Scheme 3. A full set of rate equations was defined for the side reactions as follows:

$$r_4 = k_4 c_a \quad (17)$$

$$r_5 = k_5 c_f \quad (18)$$

$$r_6 = k_6 c_a \quad (19)$$

$$r_7 = k_7 c_g \quad (20)$$

$$r_8 = k_8 c_c \quad (21)$$

$$r_9 = k_9 c_b \quad (22)$$

$$r_{10} = k_{10} c_e \quad (23)$$

$$r_{11} = k_{11} c_d \quad (24)$$

where k_i corresponds to the apparent rate constants of the reaction steps in Scheme 3. The notations for all compounds in the rate equation were as follows: a: 4-propylguaiacol, b: 4-propylphenol, c: propylbenzene, d: propylcyclohexane, e: 4-propylcyclohexene, f: 4-propylcatechol, g: 1,2-dimethoxyl-4-propylbenzene, h: 1-methyl-3-propylbenzene, and i: side products. The concentrations of propylcyclopentane, 1-methyl-2-propylcyclopentane, and 1-methyl-2-propylcyclohexane were low and consequently were lumped together as one and labeled as c_i. The complete mass balance equations for the improved kinetic model include the following:

$$\frac{dC_a}{dt} = -r_1 - r_4 - r_6 \quad (25)$$

$$\frac{dC_b}{dt} = r_1 + r_5 + r_7 - r_2 \quad (26)$$

$$\frac{dC_c}{dt} = r_2 - r_8 - r_3 - r_9 \quad (27)$$

$$\frac{dC_d}{dt} = r_3 + r_{10} - r_{11} \quad (28)$$

$$\frac{dC_e}{dt} = r_9 - r_{10} \quad (29)$$

$$\frac{dC_f}{dt} = r_4 - r_5 \quad (30)$$

$$\frac{dC_g}{dt} = r_6 - r_7 \quad (31)$$

$$\frac{dC_h}{dt} = r_8 \quad (32)$$

$$\frac{dC_i}{dt} = r_{11} \quad (33)$$

where C_a is the concentration of the initial feed (4-propylguaiacol) expressed in mol/L, C_x is the concentration of compound x (4-propylphenol or any side products) and t is the reaction time.

Subsequently, an improved model that took all side reactions into account was proposed. The kinetic fitting results for all sulfided catalysts are shown in Figure 19. The fitting results were generally improved, and the experiments agreed well with the pseudo-first-order kinetic model. The best description of the concentration profile was obtained with the sulfided NiMo catalyst, which had a 95% coefficient of determination. It was concluded that the proposed model was well described by the experimental data points and modeling results. The estimated parameters for the apparent kinetic rate constant with a 95% confidence interval are presented in Supplementary Information in Paper I. The high estimated confidence intervals could be attributed to the small experimental sets and that the parameters were highly correlated.

The current modeling results for the HDO of PG revealed that the same reaction routes can be applied to all the studied catalysts. The influence of the added transition metals was reflected in the modeling results. For instance, the results showed that adding promoters to the Mo catalyst did not change the reaction routes significantly. The rate constant k_1 represents the rate for the demethoxylation step of PG, and the Mo catalyst had the highest value ($k_1 = 1.86 \times 10^{-2}$ min^{-1}) of all the catalysts. This result explains the faster demethoxylation rate for the unpromoted Mo catalyst as compared to the others, and it can also be related to the faster initial PG conversion of the Mo catalyst during the first 1-2 h of the reaction. Besides, the kinetic rate constants k_3 (8.50×10^{-2} min^{-1}) and k_9 (9.92×10^{-2} min^{-1}) were the highest for the sulfided NiMo catalyst. These results correlate with the highest rate of the hydrogenation of propylbenzene to propylcyclohexane and propylcyclohexene given the highest yield of deoxygenated products achieved by the NiMo catalyst as shown previously (Section 4.1.1). It was found that both the CuMo and FeMo catalysts, had a lower rate constant, k_2, than the Mo catalyst, suggesting that they inhibited the dehydroxylation of 4-propylphenol. The ZnMo catalyst had a higher rate constant k_2 (1.05×10^{-2} min^{-1}) than the Mo catalyst, but a lower k_3 (1.65×10^{-2} min^{-1}) and k_9 (6.73×10^{-2} min^{-1}) rate constant relative to the Mo catalyst, hence corroborating its highest aromatics production. The lowest rate constant, k_3, for the FeMo catalyst also verified its low rate of propylbenzene hydrogenation in HDO of PG which resulted in a 16% aromatic yield at the end of the reaction.

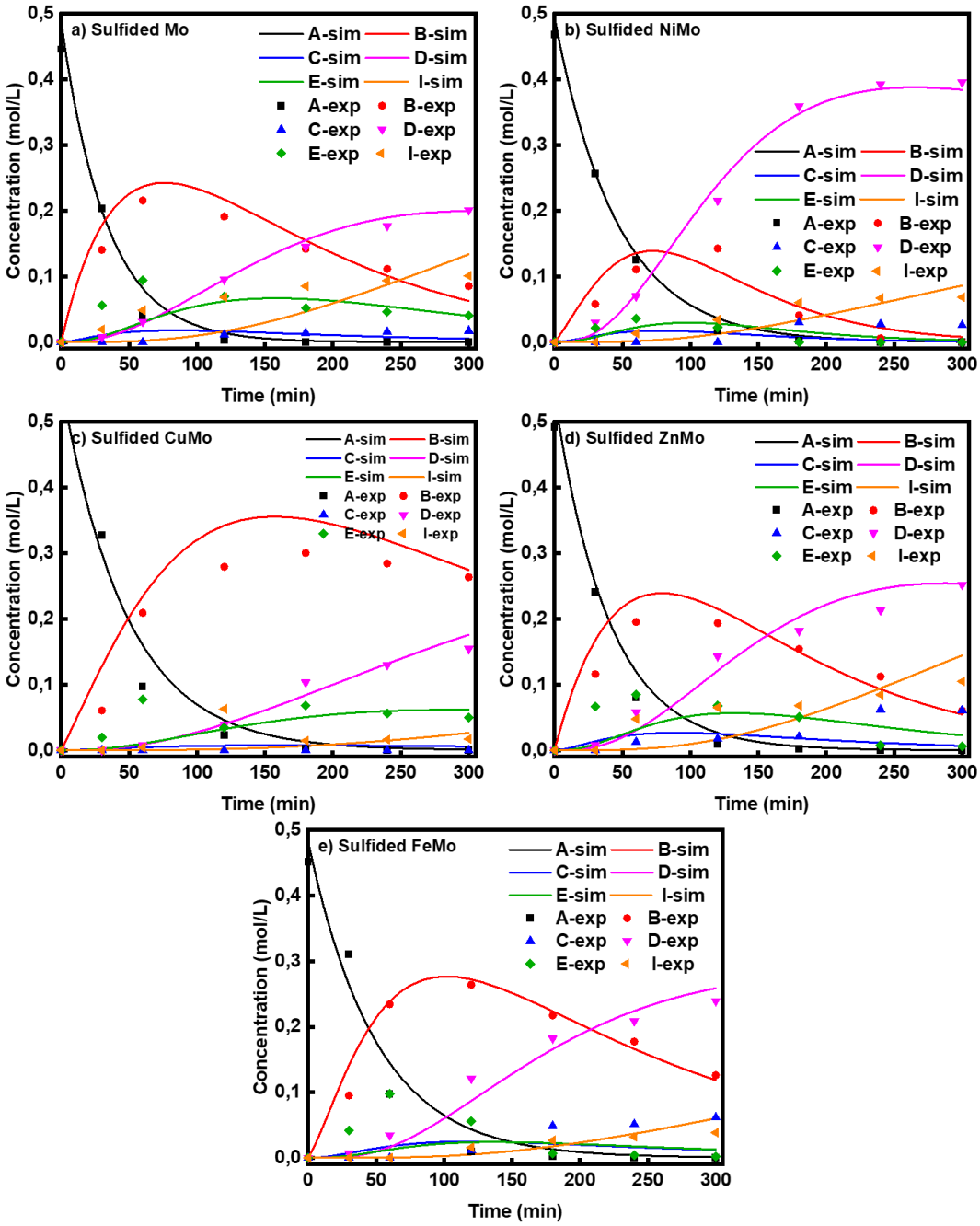

Figure 19. Kinetic fitting results for HDO of PG over sulfided a) Mo, b) NiMo, c) CuMo, d) ZnMo, and e) FeMo. The solid line denotes the modeling results and the points represent experimental data. Notation: A = PG, B = 4-propylphenol, C = propylbenzene, D = propylcyclohexane, E = propylcyclohexene, and I = side products.

4.1.4 Hydrotreatment of Kraft lignin over sulfided NiMo, ZnMo, and FeMo catalysts

4-propylguaiacol was used as a model compound for the study of HDO reaction using the Mo sulfided catalysts promoted by transition metals (Ni, Fe, Cu, and Zn) in the first study. The reason for using a model reaction was to assess the activity of the sulfided catalysts. At the same time, to study the selectivity of different sulfided catalysts for different products based on their functionalities like phenolics, deoxygenated cyclic compounds, and aromatics before investigating their activities for more complex substrates like lignin.

In order to verify the representability of PG as an appropriate model compound for more complex bio-feedstocks, the sulfided NiMo, ZnMo, and FeMo catalysts were also examined for the hydrotreatment of kraft lignin.

Figure 20 presents a comparison of different product selectivities (in terms of relative MS blob volume %) for sulfided ZnMo, FeMo, and NiMo catalysts in the hydrotreatment of kraft lignin at 340 °C and 40 bar initial H_2 pressure using the same batch reactor system as described for HDO of PG. The main focus was put on the analysis of the upgraded lignin oil and the product selectivities when using different sulfided catalysts. The reaction samples were subjected to 2D GC × GC analysis for in-depth product analysis and the respective chromatograms are shown in Supporting Information in Paper I. A diverse group of products was obtained after the hydrotreatment, such as deoxygenated aromatics and cycloalkanes, dimers, and polyaromatics, and also oxygenated compounds. A noticeable difference in selectivity for deoxygenated monomeric cycloalkanes of 26% and 13% were obtained for ZnMo and FeMo sulfided catalysts, respectively. While a 62% monomeric cycloalkane selectivity was obtained for the NiMo sulfided catalyst. The higher deoxygenation ability of the NiMo catalyst can be clarified here in the case of hydrotreatment of Kraft lignin in agreement with the results obtained from the model reaction.

Sulfided NiMo catalyst was seen to possess a higher selectivity of 12% than ZnMo (8%) and FeMo catalysts (4%) for deoxygenated monomer aromatic products. Oxygenate products, such as monomeric and dimeric phenolic compounds were found in the product samples for all the catalyst systems with FeMo (50.9%) giving the highest selectivity. The major difference in the product distribution between the model reaction and lignin hydrotreatment was the presence of dimeric and trimeric products such as naphthalenes and anthracenes in the lignin hydrotreatment experiments. This was attributed to the lignin depolymerization at the onset of the reaction yielding the monomeric, dimeric, and polymeric phenolic fragments from lignin as observed in the GC × GC analysis results. The higher deoxygenation ability of NiMo catalysts also resulted in the absence of naphthol-derived products in the product distribution after a 5 h hydrotreatment. There were also solid residue products formed after the hydrotreatment for all catalysts, however, they were not quantified in this study.

The lignin reactivity follows first the depolymerization of lignin fragments yielding compounds with hydroxyl and methoxy groups. These oxygen-contained lignin fragments further underwent different upgrading reactions like HDO and partial HDO producing deoxygenated products and alkylphenols. The use of PG as a model compound could qualitatively indicate the reactivity scale of the sulfided catalysts towards desired products and facilitate the search for the probable reaction network towards the upgrading of complex lignin compounds to different valuable products. The future work will be focused on the upgrading of lignin, including in-depth product and kinetic analysis considering the formation of larger molecules, such as dimers and trimers in biomass upgrading reactions and also solid residue products.

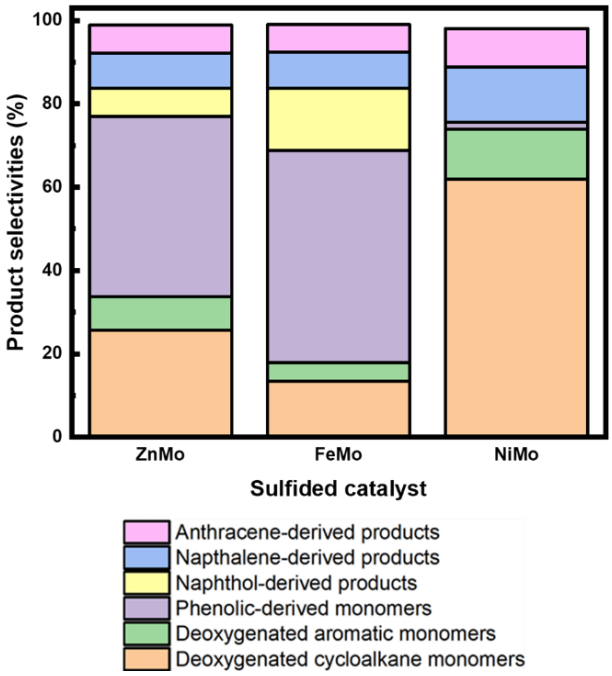

Figure 20. 2D GC × GC analysis for the comparison of detectable liquid phase product selectivities using sulfided ZnMo, FeMo, and NiMo catalysts for hydrotreatment of kraft lignin. Reaction conditions: 3:1 lignin to catalyst mass ratio, 340 ˚C, 40 bar initial H_2 pressure, 5 h, and 1000 rpm.

4.2 Annealing treatment of unsupported MoS_2 for hydrodeoxygenation of propylguaiacol and hydrotreatment of Kraft lignin

4.2.1 Hydrothermal synthesis of unsupported MoS_2 for HDO of PG

Unsupported MoS_2 catalyst was synthesized in the second study and tested in HDO of PG. The effect of the annealing treatment on the synthesized sample was investigated and found to be crucial to enhance HDO activity. The effect of hydrothermal synthesis time and the pH adjustment with the annealing treatment on the catalytic activity was studied using the model reaction. The annealed MoS_2 and bulk MoS_2 catalysts were then further evaluated in the hydrotreatment of Kraft lignin.

The effects of hydrothermal synthesis time and the annealing pretreatment were studied on the model reaction. Figure 21 shows the comparison between the annealed MoS_2 and as-synthesized MoS_2 with synthesis time of 12 h and 24 h in terms of product selectivity and PG conversion at 4 h. Increasing the synthesis time from 12 h to 24 h improved the PG conversion for the as-synthesized MoS_2 catalyst. The selectivity for deoxygenated cycloalkanes, such as propylcyclohexane and propylcyclohexene, was 27.5% and 43.4% for MoS_2-12 and MoS_2-24, respectively. While for an intermediate like propylphenol, the selectivity remained in the range of 47-48%. A 24.7% selectivity for a compound with two oxygen atoms like propylcatechol (2O compound), was found for MoS_2-12 after 4 h. Increasing the synthesis time to 24 h, decreased the selectivity of the propylcatechol (2O compound) to 8.3%.

The as-synthesized catalysts underwent additional annealing treatment at 400 °C for 2 h under a nitrogen flow. The selectivity and PG conversion after 4 h for the annealed and as-synthesized catalysts are shown in Figure 21. It can be seen in Figure 21 that both annealed catalysts (MoS_2-12a and MoS_2-24a) had the same PG conversion

after 4 h. The MoS_2-12a and MoS_2-24a had a 64% and 55% selectivity for deoxygenated cycloalkane, respectively, after 4 h. It can be seen in Figure 21 that both annealed samples had a higher selectivity for deoxygenated cycloalkanes than the as-synthesized samples. The selectivity for phenolics was also reduced for both annealed samples. Interestingly, aromatics, such as propylbenzene, were found in the annealed samples with a selectivity of 18-20%. The 2O compounds were not detected in the reaction medium using either annealed sample (MoS_2-12a and MoS_2-24a) after 4 h. The results indicate that a shorter synthesis time was better for the PG deoxygenation when using annealed catalysts. A longer synthesis time was preferable for the as-synthesized catalysts to attain better deoxygenation activity. The difference in results can be attributed to that 12 h synthesis time was enough to nucleate sufficient MoS_2 crystallites, and the annealing treatment facilitated the growth of MoS_2 crystals.

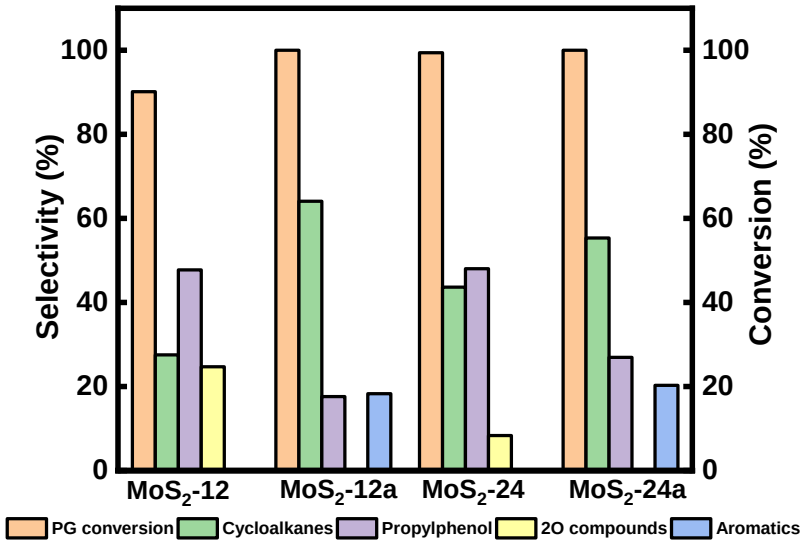

Figure 21. Comparison between selectivity for reaction product and PG conversion after 4 h for HDO of PG over MoS_2-12, MoS_2-12a, MoS_2-24, and MoS_2-24a at 50 bar total H_2 pressure, 300 °C, and 1000 rpm.

The effect of not adding acid during the synthesis of unsupported MoS_2 was investigated in the HDO of PG. The product distribution for both as-synthesized and annealed catalysts prepared without adding acid is shown in Figure 22. A final PG conversion of 86.6% was obtained after 5 h for the as-synthesized MoS_2 prepared without the addition of acid. Besides, the selectivity for 4-propylphenol increased to 42.5% after 2 h and stabilized at 40.8% after 5 h. A downward trend was found also for the selectivity for oxygenated intermediates (2O-compounds) which gave a final selectivity of 19.5% (Figure 22a). A gradual increase in the selectivity for deoxygenated cycloalkanes was found, which gave a final selectivity of 40%. For a fair comparison, the fresh as-synthesized MoS_2 (without acid addition) underwent an annealing treatment similar to the one described previously (Section 3.1.2) and was applied in the HDO of PG. Surprisingly, the annealing treatment had a negative effect on the PG conversion, showing a final PG conversion of 74.2% (Figure 22b). In contrast, a slight increase in the selectivity for deoxygenated cycloalkanes selectivity was found, which gave a final selectivity of 46.6% (Figure 22b). A decreasing trend was found for the selectivity for phenolics with reaction time, which gave 36.6% selectivity for 4-propylphenol and 15.8% selectivity for 4-propylcatechol (2O-compounds) after 5 h. The clear difference in the product distribution of the HDO of PG between the unsupported MoS_2 catalysts prepared with and without the

addition of acid shows that an acidic environment while synthesizing unsupported MoS_2 is crucial to produce MoS_2 with a smaller particle size (evident in SEM images, Figure 25). The resulting MoS_2 particle size had a direct effect on the HDO selectivity. This result is in line with the conclusion by Zhang et. al[91], which shows that higher HDS and hydrogenation activities can be achieved using MoS_2 prepared with low pH values. The smaller MoS_2 particles synthesized in an acidic environment had more active sites, which led to higher selectivity for HDO. It is worth mentioning that the annealing treatment proposed in this study positively enhanced the PG HDO activity when MoS_2 catalysts prepared with pH adjustment were used. The MoS_2 prepared without any pH adjustment had the opposite effect, especially on the PG conversion, and did not facilitate the growth of MoS_2 crystals.

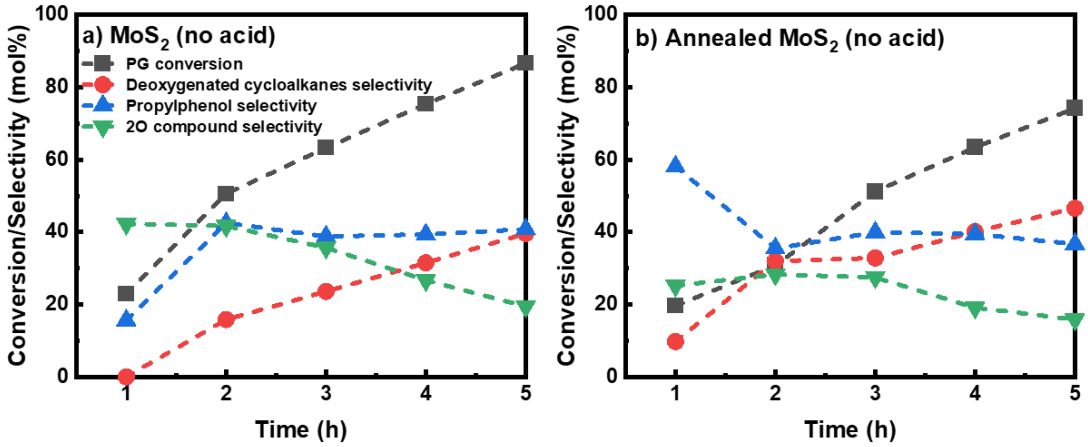

Figure 22. Reaction product distribution for HDO of PG over a) MoS_2 prepared without acid adjustment and b) annealed MoS_2 without acid adjustment at 50 bar total H_2 pressure, 300 ˚C and 1000 rpm.

4.2.2 Catalyst characterization

The specific surface area, pore volume, and pore size of the unsupported MoS_2 and bulk MoS_2 catalysts are listed in Table 8. The specific surface area of the catalysts was ranked in decreasing order: MoS_2-24a > MoS_2-12a > MoS_2-24 > MoS_2-12 > bulk MoS_2. It was found that prolonging the synthesis time from 12 h to 24 h had a negligible effect on the specific surface area of the catalyst, and gave a range between 15-16 m^2g^{-1} for MoS_2-12 and MoS_2-24. In contrast, both annealed samples (MoS_2-12a and MoS_2-24a) gave a higher specific surface area than the as-synthesized catalysts. The N_2 adsorption-desorption isotherms for all the catalysts are provided in Supporting Information in Paper II. The isotherms for the annealed MoS_2 catalysts were characterized as type IV isotherms according to the IUPAC classification[92]. A prominent H3 type hysteresis loop was also found for both annealed MoS_2 samples. This loop featured slit-shaped pores created by the build-up of MoS_2 layers. The as-synthesized and bulk MoS_2 type-II isotherms had a distinctive form indicating a non-porous character. This observation can be explained by the agglomeration of particles that formed larger lumped particles with reduced porosity, as shown in the SEM images (Figure 25). These findings suggest that an annealing treatment can significantly increase the specific surface area and the porosity of the as-synthesized catalysts. It is important to highlight that this porosity was created by the shrinkage of particles during annealing and the resulting formation of MoS_2 crystals (see the XRD analysis, Figure 23a)). They were re-coordinated and agglomerated to generate cavities. It is also worth noting that MoS_2-12a had the highest pore volume and the lowest pore size of all the unsupported catalysts.

Table 8. Physical properties (surface area, pore-volume, and pore size) of synthesized unsupported catalysts.

Catalysts	Surface area (m^2/g)	Pore volume (cm^3/g)	Pore size (Å)
MoS_2-12	15.4	0.34	108
MoS_2-12a	27.8	0.60	83.8
MoS_2-24	16.2	0.13	317
MoS_2-24a	37.1	0.11	105
Bulk MoS_2	4.70	0.03	177

Figure 23a) shows the XRD diffractograms for the MoS_2 unsupported catalysts. The XRD patterns show that the as-synthesized samples had low crystallinity with a peak at $2\theta = 14°$, representing the typical (002) plane of hexagonal MoS_2. The results also confirm that prolonging the synthesis time from 12 h to 24 h did not improve the crystallinity of the samples resulted in the same XRD pattern (Figure 23). Prominent peaks were visible at $2\theta = 14°$, 33°, 39°, and 59° for both annealed MoS_2 catalysts attributed to the (002), (100), (103), and (110) planes of MoS_2[93]. The improved crystallinity of the as-synthesized MoS_2 after a simple annealing treatment suggests that the annealing process at 400 °C for 2 h can promote the growth of MoS_2 crystals. In comparison, the bulk MoS_2 was highly crystalline, as shown in Figure 23a).

Raman spectroscopy was performed to understand the chemical state of the as-synthesized and annealed catalysts. The Raman spectra of MoS_2-24 and MoS_2-24a were obtained at the 532 nm CW laser excitation mark with an average power of 0.3 mW, as shown in Figure 23b). For MoS_2-24a catalysts, four main Raman peaks located at 379 cm^{-1} (E^1_{2g}), 404 cm^{-1} (A_{1g}), 283 cm^{-1} (E_{1g}) and 454 cm^{-1} (E_{1g}) indicate that the usual 2H-MoS_2 phase was present[94]. Two low-intensity Raman peaks at 219 cm^{-1} and 335 cm^{-1} were identified in the spectra for MoS_2-24a, proving the existence of the 1T phase of MoS_2[94]. The results indicate that the annealing pre-treatment changed the structure of the as-synthesized catalysts and resulted in mixed 1T and 2H phases for MoS_2. In contrast, for MoS_2-24 catalysts, three peaks were identified, as shown in Figure 23b) with a relatively lower intensity. This proves the lower crystallinity of the as-synthesized catalyst. The results from Raman spectroscopy analysis corroborate with the results obtained from XRD analysis.

The chemical state and composition of the unsupported MoS_2 catalysts before and after the annealing treatment were determined with XPS (Figure 24). The Mo 3d spectra in Figure 24a) and Figure 24c) were deconvoluted into three Mo $3d_{5/2}$ – Mo $3d_{3/2}$ doublets for the as-synthesized samples. The presence of the Mo^{4+} oxidation state indicated by two characteristic peaks at 229.3 eV and 232.5 eV binding energies, proved the existence of the MoS_2 species[95]. Characteristic peaks at the binding energies 230.0 eV and 233.0 eV were found for the Mo^{5+} oxidation state, which demonstrated the presence of intermediate oxysulfide species (MoO_xS_y) in the as-synthesized catalysts[96]. An additional doublet at 233.4 eV and 235.8 eV associated with the Mo^{6+} oxidation state which is associated with the MoO_3 species was also found[97]. Table 9 shows the Mo 3d composition of the Mo states obtained from the XPS data. The sulfidation degree based on the Mo^{4+} content increased for both annealed MoS_2 more than for the as-synthesized unsupported catalysts. MoS_2-24a had the highest degree and correspondingly lowest degree of oxidation of Mo. The presence of oxysulfide species in the as-synthesized catalysts was caused by one of the reactions that are expected to occur during the synthesis of MoS_2, where $(NH_4)_6Mo_7O_{24}$ reacts with H_2S and forms MoO_xS_y, ammonia, and water. However, no oxysulfide species were found in either annealed catalysts. This

finding suggests that the MoO_xS_y phase may have been completely converted into MoS_3, and the annealing pretreatment facilitated the thermal decomposition of MoS_3 to MoS_2.

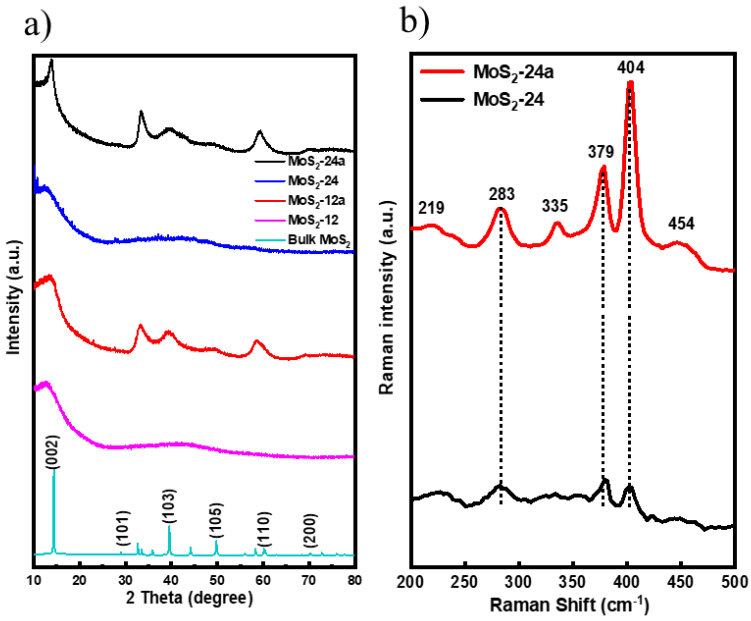

Figure 23. a) XRD patterns for MoS_2-12, MoS_2-12a, MoS_2-24, MoS_2-24a and bulk MoS_2 and b) Raman spectra for MoS_2-24 and MoS_2-24a catalysts.

Table 9 Mo 3d composition for MoS_2-12, MoS_2-12a, MoS_2-24, and MoS_2-24a.

Catalyst	Mo 3d composition (area %)		
	Mo^{4+}	Mo^{5+}	Mo^{6+}
MoS_2-12	62.9	22.2	14.9
MoS_2-12a	88.6	-	11.4
MoS_2-24	82.9	11.3	5.8
MoS_2-24a	93.1	-	6.9

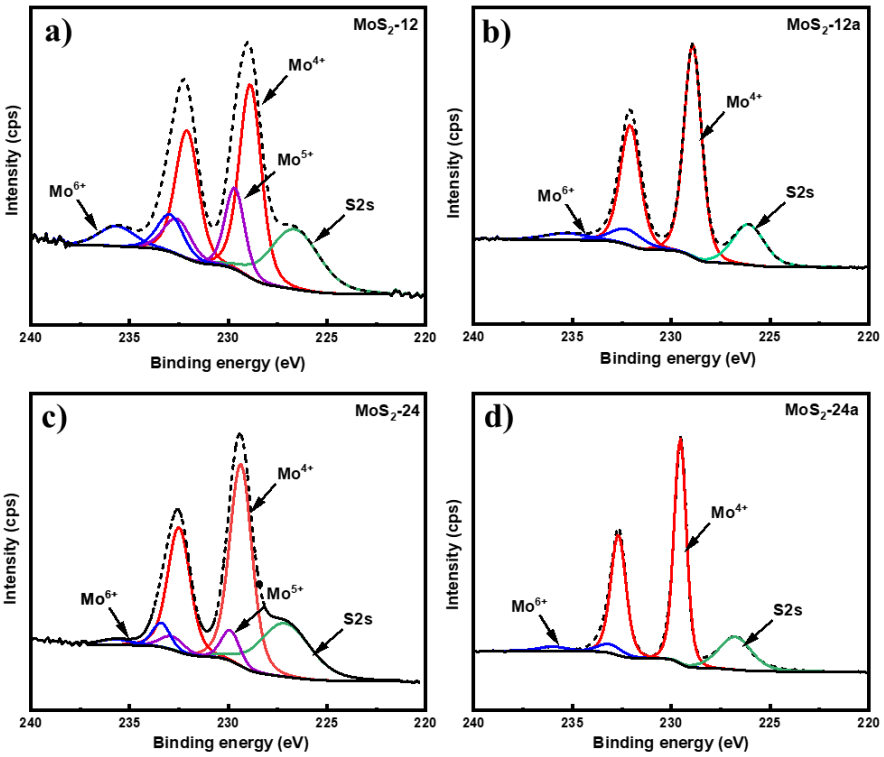

Figure 24. XPS spectra of Mo 3d for a) MoS_2-12, b) MoS_2-12a, c) MoS_2-24, and d) MoS_2-24a.

The structure and morphologies of the unsupported catalysts synthesized in this work were examined with SEM. The laminar growth of the MoS_2 during hydrothermal synthesis resulted in the formation of spherical particle agglomerates, shown in the SEM images in Figure 25. The average particle diameter was measured based on all the SEM images using ImageJ software. The distribution of particle size is shown in the insets of Figure 25. As can be seen in Figure 25(e) and Figure 25(f), the MoS_2-24 catalyst consisted of a mixture of larger and smaller particles with an average particle diameter of 305 nm. Similar morphology was found for MoS_2-12 (Figure 25(a) and (b)). The MoS_2-24a catalyst had more dispersed and uniformly distributed MoS_2 particles than the as-synthesized catalyst with a smaller average particle diameter of 190 nm as shown in the SEM images in Figure 25(g) and (h). In general, the annealed catalysts had a more defined morphology. The SEM analysis also showed that the annealing treatment reduced the MoS_2 particle diameter and size distribution of particles.

To understand the effect of pH adjustment during synthesis on the morphology of the MoS_2 catalyst, a batch of unsupported MoS_2 was prepared following the same procedure but omitting the acid adjustment step, as described in Section 3.1.2. The subsequent batch was then examined with SEM, and the results are shown in Figure 26. The particles in Figure 26 show an apparent flower-like morphology with a larger average particle diameter of 2 µm. It is worth noting that this is almost the average particle size for the bulk MoS_2 sample (6 µm, max 40 µm). The characterization results presented here are also in line with the findings by Zhang et. al[91]. The pH adjustment step in the catalyst synthesis was important to facilitate the growing of MoS_2 micelles, which eventually formed smaller crystallites in the MoS_2 catalysts (Figure 25 and Figure 26). A material with a larger particle size was formed for the MoS_2 catalyst prepared without acid addition (Figure 26).

High-resolution transmission electron microscopy (HRTEM) was also performed to better understand the effect of annealing on the structure of an unsupported catalyst, and the images are presented in Figure 27. The usual thread-like fringes with an interplanar distance of 0.64 nm, corresponding to the (0 0 2) basal planes of the MoS_2 catalysts, were identified in all of the HRTEM images. One of the main differences was from the HRTEM images for the annealed catalysts in which the edges showed a spiky feature that was not visible in the as-synthesized catalysts, see Figure 27. The changes in the structure near the edges of the catalyst after the annealing process could be due to the enhancement of the growth of the smaller MoS_2 crystallites in the as-synthesized catalysts. This demonstrates the importance of the annealing treatment in changing the structure of the catalysts. Consequently, the spiky edges of the annealed unsupported catalysts contributed to their higher specific surface area and the exposure of more active sites to the HDO reaction.

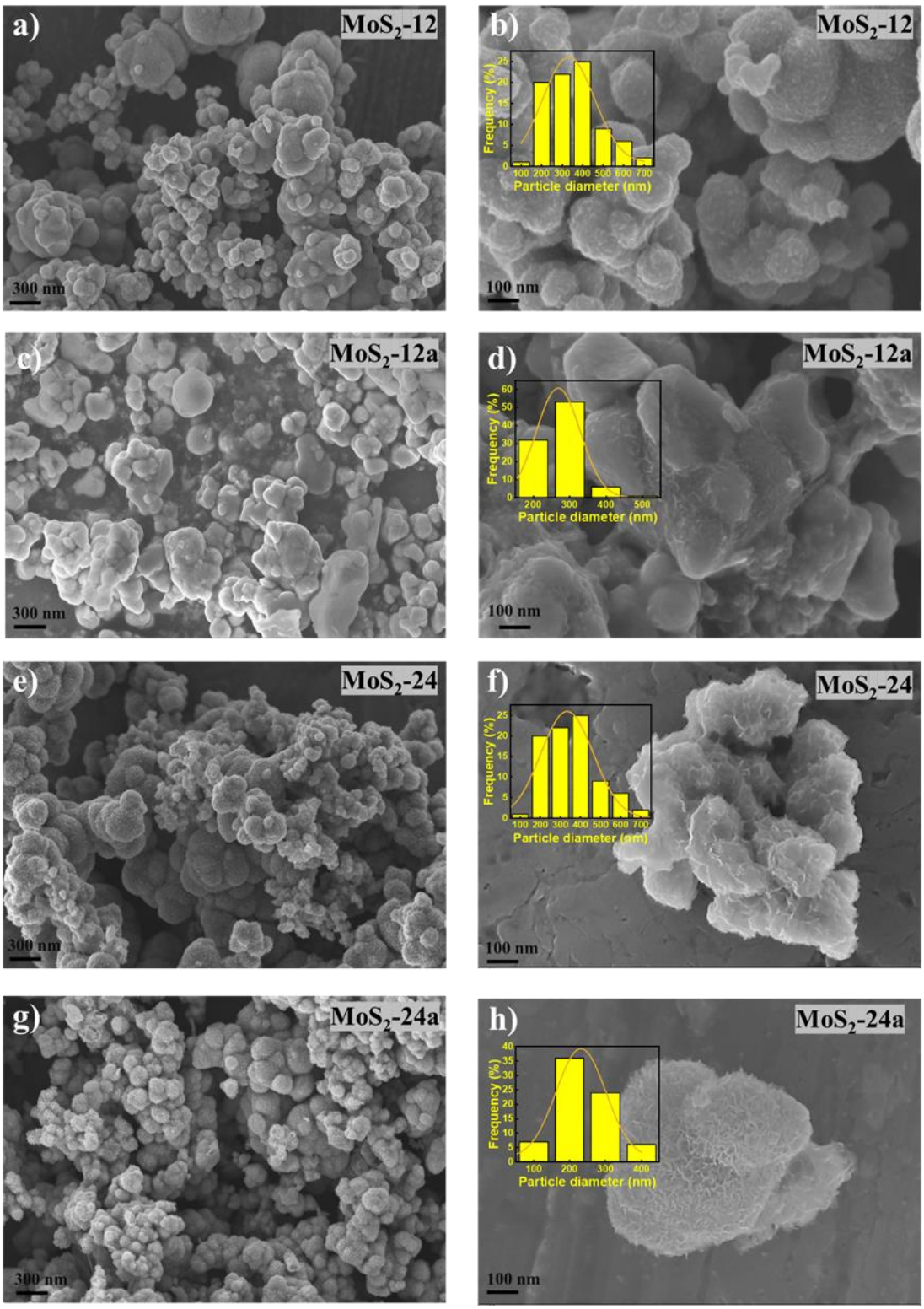

Figure 25. SEM images of (a and b) MoS_2-12, (c and d) MoS_2-12a, (e and f) MoS_2-24, and (g and h) MoS_2-24a.

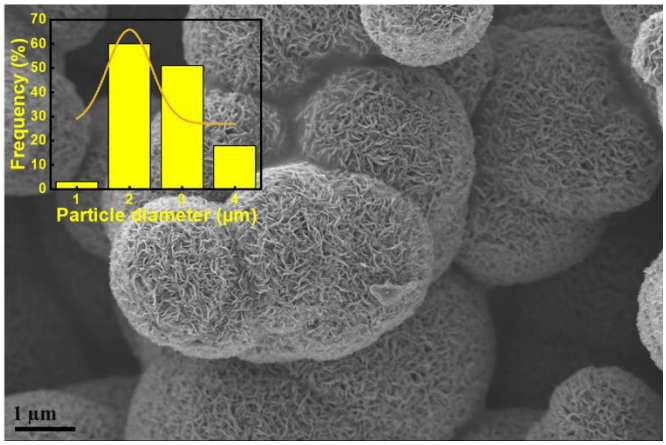

Figure 26. SEM image of MoS_2 prepared without pH adjustment.

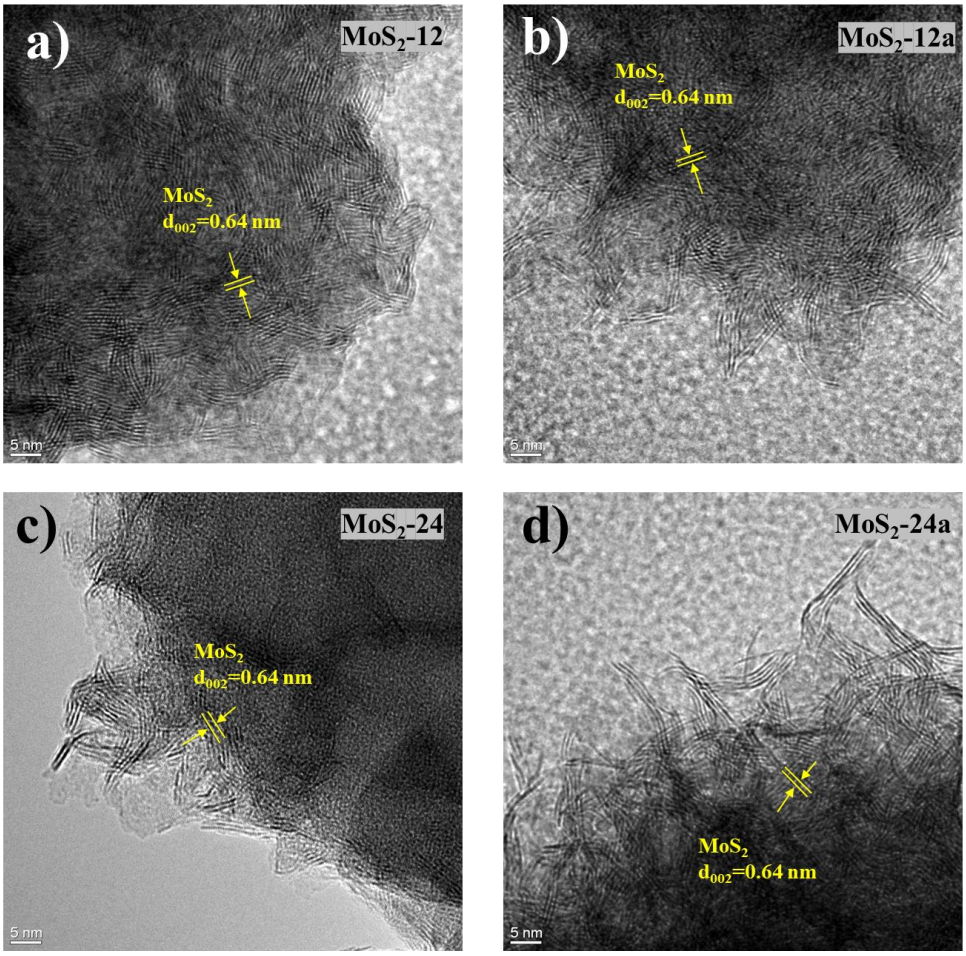

Figure 27. HRTEM images of a) MoS_2-12, b) MoS_2-12a, c) MoS_2-24, and d) MoS_2-24a.

4.2.3 Kraft lignin hydrotreatment over unsupported MoS_2 and bulk MoS_2

Both MoS_2-12a and bulk MoS_2 were tested in the hydrotreatment of Kraft lignin at 340 and 40 bar initial H_2 pressure for 5 h. The focus was on an in-depth analysis of the hydrotreated lignin oil fraction and quantifying its main product groups. Kraft lignin was found to be fully converted after 5 h for both unsupported catalysts. A comparison between the product selectivities and char yield for both catalysts is shown in Figure 29. A noticeable

difference between the product selectivities of the upgraded lignin oil fractions was found for both unsupported MoS_2 catalysts. An array of products, such as lignin monomers and dimers, were detected. These came from the depolymerization of lignin during the hydrotreatment. Figure 28 presents the major products that were found in the GC spectra for bulk MoS_2 (blue line) and MoS_2-12a (black line). The major compounds identified in the lignin oil fractions for MoS_2-12a included deoxygenated compounds like methylcyclopentane, cyclohexane, methylcyclohexane, ethylcyclopentane, ethylcyclohexane, and propylbenzene. These deoxygenated cycloalkanes and aromatics had a total selectivity of 78.6% and 20%, respectively. In contrast, for hydrotreatment using bulk MoS_2, mainly oxygenates such as guaiacol, cresol, 4-ethyl-2methoxyphenol, and propylguaiacol were found, as shown in the GC spectra in Figure 28. A total selectivity of 90.5% for these phenolic-derived compounds and 8.3% of deoxygenated cycloalkanes was obtained when bulk MoS_2 was used. The formation of solid char derived from the re-polymerization or condensation of lignin fragments was found in both cases. However, the char yield was relatively less for the MoS_2-12a catalyst than for the bulk MoS_2, as shown in Figure 29. This indicates that a catalyst with high hydrogenation and deoxygenation activity could suppress the formation of char.

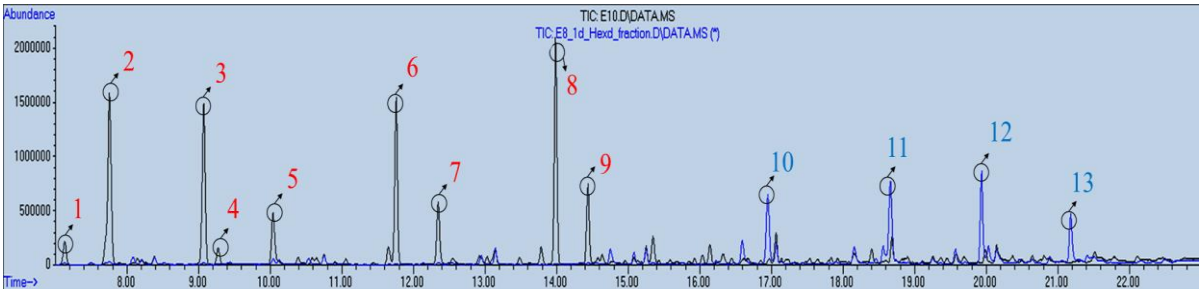

Figure 28. GC spectrum of the lignin fraction obtained from the hydrotreatment of Kraft lignin over bulk MoS_2 (blue line) and MoS_2-12a (black line). Reaction conditions: 3:1 lignin to catalyst ratio, 340 ˚C, 40 bar initial H_2 pressure, and 1000 rpm. The major compounds are labeled in the spectrum as (1) Methylcyclopentane, (2) Cyclohexane, (3) Methylcyclohexane, (4) Ethylcyclopentane, (5) Toluene, (6) Ethylcyclohexane, (7) 1,3-dimethylbenzene, (8) Propylcyclohexane, (9) Propylbenzene, (10) Guaiacol, (11) Creosol, (12) 4-ethyl-2-methoxyphenol, and (13) Propylguaiacol.

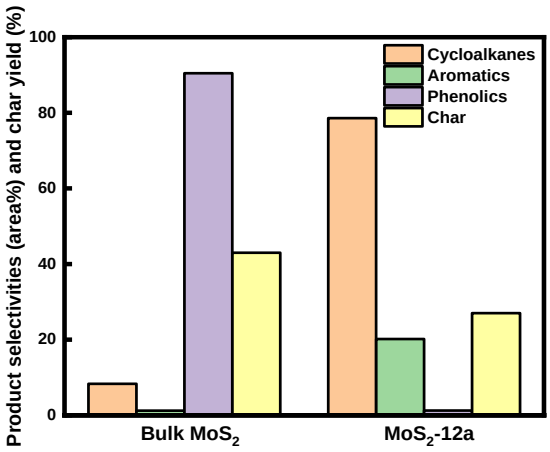

Figure 29. GCMS analysis to compare product selectivities and char yield between bulk MoS_2 and MoS_2-12a from hydrotreatment of kraft lignin. Reaction conditions: 3:1 lignin to catalyst mass ratio, 340 ˚C, 40 bar initial H_2 pressure, 5 h, and 1000 rpm.

5 Conclusions

The conclusions are based on the analyses of supported and unsupported MoS_2 in the hydrodeoxygenation of propylguaiacol and hydrotreatment of Kraft lignin.

The effect of the impregnation of the transition metals Ni, Cu, Zn, and Fe on sulfided Mo-based alumina-supported catalysts on PG conversion, and the selectivities for phenolics, deoxygenated aromatics, and cycloalkanes were studied. The impregnation of Ni, Fe, Cu, and Zn into Mo catalysts lowered the rate of demethoxylation, which gave a decrease in the initial PG conversion in the order Mo > ZnMo > CuMo > FeMo > NiMo.

The sulfided NiMo-supported catalyst gave a final yield of 94% for deoxygenated cycloalkanes. In contrast, final deoxygenated cycloalkane yields of 58.1%, 67.2%, and 44.4% were obtained for FeMo-, ZnMo-, and CuMo-supported catalysts, respectively. The deoxygenated cycloalkane yields for the non-promoted Mo-sulfided catalyst were 70%. The results show that Ni promoted the Mo catalyst while impregnating metals, such as Fe, Zn, and Cu, which inhibited the formation of deoxygenated cycloalkanes. Interestingly, the selectivity of deoxygenated aromatics increased at higher PG conversion following the order: ZnMo > FeMo > Mo > NiMo > CuMo, with 16% and 19% aromatics for ZnMo and FeMo catalysts, respectively. Both Zn and Fe had an adverse effect on the HDO activity of PG but changed the selectivity towards aromatics, such as propylbenzene, at full PG conversion. Moreover, a pseudo-first-order kinetic modeling analysis was done for PG HDO, and the model clarified the deoxygenation routes and reaction network. The inclusion of side reactions also improved the model and explained the experimental results, with more than a 90% coefficient of determination for all catalysts. The direct deoxygenation of PG was the major pathway for the removal of oxygen-containing groups with 4-propylphenol being the major intermediate. Hence, the model shows that the proposed reaction routes can be adapted for all the studied catalysts. The influence of promoters on the Mo catalysts is also be indicated in the modeling for HDO of PG. For instance, NiMo catalysts show high hydrogenation rates of aromatic rings yielding cycloalkanes. In contrast, Fe- and Mo- promoted catalysts inhibited the hydrogenation of the aromatic ring and facilitated the formation of aromatics. The current results are essential to understanding the reaction mechanism for the HDO of oxygen-containing compounds that can largely be found in biomass-derived feedstock using sulfided catalysts. The results obtained from the hydrotreatment of Kraft lignin correlate with the activity from the HDO of PG.

A simple hydrothermal synthesis method for the preparation of unsupported MoS_2 catalyst was explored in the second study. An annealing pretreatment of as-synthesized MoS_2 unsupported catalysts was found to be important to enhance the HDO activity of PG. The unsupported catalysts that had been synthesized for 12 h coupled with pH adjustment and annealing treatment gave the highest degree of deoxygenation of all the catalysts. Creating an acidic environment during catalyst synthesis was found to be important in assisting the micelles growing of MoS_2 catalyst, forming smaller particles that could influence HDO activity. A comparison was made between the HDO of PG and Kraft lignin hydrotreatment using our in-house synthesized MoS_2 and s sample of bulk MoS_2 used as catalysts. The results showed that the annealed MoS_2 unsupported catalysts gave high deoxygenation of Kraft lignin. These results also indicated that high-deoxygenation and hydrogenation catalysts could suppress the formation of char and result in a higher yield of bio-oil.

6 Future work

It was found that the unsupported TMS had good catalytic activity in the HDO reaction and the hydrotreatment of Kraft lignin. The unsupported catalysts with good hydrogenation and HDO activity also played a role in suppressing char formation reactions. More exploratory work focusing on the synthesis of unsupported TMS and the application of these unsupported TMS in upgrading Kraft lignin is an important area. An interesting future direction is also to develop a lumped kinetic model that takes into account the depolymerization of lignin producing different lignin fragments and further upgrading using unsupported TMS. Parameter optimization such as process temperature, pressure, time, and lignin-catalyst ratio for lignin hydrotreatment is important for upcoming work. Moreover, special attention should be made to understand the char formation reactions and also ways to suppress such reactions to reach minimum char yield. The characterization of solid residues resulting from the hydrotreatment is of high interest to fully understand the composition of the produced solid.

7 References

(1) Total Greenhouse Gas Emission Trends and Projections in Europe. European Environment Agency. **2020.**

(2) Greenhouse Gas Emissions from Transport in Europe — European Environment Agency. **2018**, 1–7.

(3) Chakar, F. S.; Ragauskas, A. J. Review of Current and Future Softwood Kraft Lignin Process Chemistry. *Ind. Crops Prod.* **2004**, *20* (2), 131–141.

(4) Lundberg, V. Chemical and Biochemical Biorefineries in Kraft Pulp Mills – Process Integration and Economics for Three Concepts; **2014**.

(5) Patel, M.; Kumar, A. Production of Renewable Diesel through the Hydroprocessing of Lignocellulosic Biomass-Derived Bio-Oil: A Review. *Renew. Sustain. Energy Rev.* **2016**, *58*, 1293–1307.

(6) Mäki-Arvela, P.; Murzin, D. Hydrodeoxygenation of Lignin-Derived Phenols: From Fundamental Studies towards Industrial Applications. *Catalysts* **2017**.

(7) Furimsky, E. Catalytic Hydrodeoxygenation. *Applied Catalysis* **2000**, *199*, 147–190.

(8) Prasomsri, T.; Shetty, M.; Murugappan, K.; Román-Leshkov, Y. Insights into the Catalytic Activity and Surface Modification of MoO_3 during the Hydrodeoxygenation of Lignin-Derived Model Compounds into Aromatic Hydrocarbons under Low Hydrogen Pressures. *Energy Environ. Sci.* **2014**, *7* (8), 2660–2669.

(9) Jin, S.; Xiao, Z.; Li, C.; Chen, X.; Wang, L.; Xing, J.; Li, W.; Liang, C. Catalytic Hydrodeoxygenation of Anisole as Lignin Model Compound over Supported Nickel Catalysts. *Catal. Today* **2014**, *234*, 125–132.

(10) Kohli, K.; Prajapati, R.; Maity, S. K.; Sharma, B. K. Effect of Silica, Activated Carbon, and Alumina Supports on NiMo Catalysts for Residue Upgrading. *Energies* **2020**, *13* (18), 1–16.

(11) Mukundan, S.; Atanda, L.; Beltramini, J. Thermocatalytic Cleavage of C-C and C-O Bonds in Model Compounds and Kraft Lignin by $NiMoS_2$/C Nanocatalysts. *Sustain. Energy Fuels* **2019**, *3* (5), 1317–1328.

(12) Mukundan, S.; Chowdari, R. K.; Beltramini, J. External Solvent-Free Catalytic Hydrodeoxygenation of Softwood Lignin to Aromatics over Carbon–ZrO_2 Supported Ni/MoS_2 Catalysts. *Adv. Sustain. Syst.* **2020**, *2000243*, 1–12.

(13) Wang, L.; Xiao, F. S. Nanoporous Catalysts for Biomass Conversion. *Green Chem.* **2015**, *17* (1), 24–39.

(14) Eijsbouts, S.; Mayo, S. W.; Fujita, K. Unsupported Transition Metal Sulfide Catalysts: From Fundamentals to Industrial Application. *Appl. Catal. A Gen.* **2007**, 322, 58–6.

(15) Plantenga, F. L.; Cerfontain, R.; Eijsbouts, S.; Houtert, F. Van; Anderson, G. H.; Miseo, S.; Soled, S.; Riley, K.; Fujita, K.; Inoue, Y.; " NEBULA ": A Hydroprocessing Catalyst with Breakthrough Activity. **2003**, 846–849.

(16) Bellussi, G.; Rispoli, G.; Landoni, A.; Millini, R.; Molinari, D.; Montanari, E.; Moscotti, D.; Pollesel, P. Hydroconversion of Heavy Residues in Slurry Reactors: Developments and Perspectives. *J. Catal.* **2013**,

308, 189–200.

(17) Bergvall, N.; Sandström, L.; Weiland, F.; Öhrman, O. G. W. Corefining of Fast Pyrolysis Bio-Oil with Vacuum Residue and Vacuum Gas Oil in a Continuous Slurry Hydrocracking Process. *Energy and Fuels* **2020**, *34* (7), 8452–8465.

(18) Mattsson, C.; Andersson, S. I.; Belkheiri, T.; Åmand, L. E.; Olausson, L.; Vamling, L.; Theliander, H. Using 2D NMR to Characterize the Structure of the Low and High Molecular Weight Fractions of Bio-Oil Obtained from LignoBoost™ Kraft Lignin Depolymerized in Subcritical Water. *Biomass and Bioenergy* **2016**, *95*, 364–377.

(19) Resende, F. L. P.; Fraley, S. A.; Berger, M. J.; Savage, P. E. Noncatalytic Gasification of Lignin in Supercritical Water. *Energy and Fuels* **2008**, *22* (2), 1328–1334.

(20) Demirbaş, A. Effect of Lignin Content on Aqueous Liquefaction Products of Biomass. *Energy Convers. Manag.* **2000**, *41* (15), 1601–1607.

(21) Doherty, W. O. S.; Mousavioun, P.; Fellows, C. M. Value-Adding to Cellulosic Ethanol: Lignin Polymers. *Ind. Crops Prod.* **2011**, *33* (2), 259–276.

(22) García-Mendoza, C.; Santolalla-Vargas, C. E.; Woolfolk, L. G.; del Ángel, P.; de los Reyes, J. A. Effect of TiO_2 in Supported NiWS Catalysts for the Hydrodeoxygenation of Guaiacol. *Catal. Today* **2020**.

(23) Hong, Y. K.; Lee, D. W.; Eom, H. J.; Lee, K. Y. The Catalytic Activity of Sulfided Ni/W/TiO_2 (Anatase) for the Hydrodeoxygenation of Guaiacol. *J. Mol. Catal. A Chem.* **2014**, *392*, 241–246.

(24) Tavizón-Pozos, J. A.; Suárez-Toriello, V. A.; Del Ángel, P.; De Los Reyes, J. A. Hydrodeoxygenation of Phenol over Sulfided CoMo Catalysts Supported on a Mixed Al_2O_3-TiO_2 Oxide. *Int. J. Chem. React. Eng.* **2016**, *14* (6), 1211–1223.

(25) Ferrari, M.; Bosmans, S.; Maggi, R.; Delmon, B.; Grange, P. CoMo/Carbon Hydrodeoxygenation Catalysts: Influence of the Hydrogen Sulfide Partial Pressure and of the Sulfidation Temperature. *Catal. Today* **2001**, *65* (2–4), 257–264.

(26) Ruiz, P. E.; Frederick, B. G.; Sisto, W. J. De; Austin, R. N.; Radovic, L. R.; Leiva, K.; García, R.; Escalona, N.; Wheeler, M. C. Guaiacol Hydrodeoxygenation on MoS_2 Catalysts : Influence of Activated Carbon Supports. **2012**, *27*, 44–48.

(27) Mukundan, S.; Konarova, M.; Atanda, L.; Ma, Q.; Beltramini, J. Guaiacol Hydrodeoxygenation Reaction Catalyzed by Highly Dispersed, Single Layered MoS_2/C. *Catal. Sci. Technol.* **2015**, *5* (9), 4422–4432.

(28) Templis, C. C.; Revelas, C. J.; Papastylianou, A. A.; Papayannakos, N. G. Phenol Hydrodeoxygenation over a Reduced and Sulfided NiMo/γ-Al_2O_3 Catalyst. *Ind. Eng. Chem. Res.* **2019**, *58* (16), 6278–6287.

(29) Badawi, M.; Paul, J. F.; Payen, E.; Romero, Y.; Richard, F.; Brunet, S.; Popov, A.; Kondratieva, E.; Gilson, J. P.; Mariey, L. Hydrodésoxygénation de Composés Phénoliques En Présence de Catalyseurs Sulfurés (Co)Mo/Al_2O_3: Une Étude Expérimentale et Théorique. *Oil Gas Sci. Technol.* **2013**, *68* (5), 829–840.

(30) Romero, Y.; Richard, F.; Brunet, S. Hydrodeoxygenation of 2-Ethylphenol as a Model Compound of Bio-Crude over Sulfided Mo-Based Catalysts: Promoting Effect and Reaction Mechanism. *Appl. Catal. B Environ.* **2010**, *98* (3–4), 213–223.

(31) Yang, Y.; Gilbert, A.; Xu, C. (Charles). Hydrodeoxygenation of Bio-Crude in Supercritical Hexane with Sulfided CoMo and CoMoP Catalysts Supported on MgO: A Model Compound Study Using Phenol. *Appl. Catal. A Gen.* **2009**, *360* (2), 242–249.

(32) Leiva, K.; Martinez, N.; Sepulveda, C.; García, R.; Jiménez, C. A.; Laurenti, D.; Vrinat, M.; Geantet, C.; Fierro, J. L. G.; Ghampson, I. T. Hydrodeoxygenation of 2-Methoxyphenol over Different Re Active Phases Supported on SiO_2 Catalysts. *Appl. Catal. A Gen.* **2015**, *490*, 71–79.

(33) Leiva, K.; Sepúlveda, C.; García, R.; Fierro, J. L. G.; Escalona, N. Effect of Water on the Conversions of 2-Methoxyphenol and Phenol as Bio-Oil Model Compounds over ReS_2/SiO_2 Catalyst. *Catal. Commun.* **2014**, *53*, 33–37.

(34) Sepúlveda, C.; García, R.; Reyes, P.; Ghampson, I. T.; Fierro, J. L. G.; Laurenti, D.; Vrinat, M.; Escalona, N. Hydrodeoxygenation of Guaiacol over ReS_2/Activated Carbon Catalysts. Support and Re Loading Effect. *Appl. Catal. A Gen.* **2014**, *475*, 427–437.

(35) Ruiz, P. E.; Leiva, K.; Garcia, R.; Reyes, P.; Fierro, J. L. G.; Escalona, N. Relevance of Sulfiding Pretreatment on the Performance of Re/ZrO_2 and Re/ZrO_2-Sulfated Catalysts for the Hydrodeoxygenation of Guayacol. *Appl. Catal. A Gen.* **2010**, *384* (1–2), 78–83.

(36) Sepúlveda, C.; Escalona, N.; García, R.; Laurenti, D.; Vrinat, M. Hydrodeoxygenation and Hydrodesulfurization Co-Processing over ReS_2 Supported Catalysts. *Catal. Today* **2012**, *195* (1), 101–105.

(37) Infantes-Molina, A.; Pawelec, B.; Fierro, J. L. G.; Loricera, C. V.; Jiménez-López, A.; Rodríguez-Castellón, E. Effect of Ir and Pt Addition on the HDO Performance of RuS_2/SBA-15 Sulfide Catalysts. *Top. Catal.* **2015**, *58* (4–6), 247–257.

(38) Jongerius, A. L.; Jastrzebski, R.; Bruijnincx, P. C. A.; Weckhuysen, B. M. CoMo Sulfide-Catalyzed Hydrodeoxygenation of Lignin Model Compounds: An Extended Reaction Network for the Conversion of Monomeric and Dimeric Substrates. *J. Catal.* **2012**, *285* (1), 315–323.

(39) Şenol, O. I.; Ryymin, E. M.; Viljava, T. R.; Krause, A. O. I. Effect of Hydrogen Sulphide on the Hydrodeoxygenation of Aromatic and Aliphatic Oxygenates on Sulphided Catalysts. *J. Mol. Catal. A Chem.* **2007**, *277* (1–2), 107–112.

(40) Gutierrez, A.; Turpeinen, E. M.; Viljava, T. R.; Krause, O. Hydrodeoxygenation of Model Compounds on Sulfided $CoMo/\gamma\text{-}Al_2O_3$ and $NiMo/\gamma\text{-}Al_2O_3$ Catalysts; Role of Sulfur-Containing Groups in Reaction Networks. *Catal. Today* **2017**, *285*, 125–134.

(41) Ryymin, E. M.; Honkela, M. L.; Viljava, T. R.; Krause, A. O. I. Competitive Reactions and Mechanisms in the Simultaneous HDO of Phenol and Methyl Heptanoate over Sulphided $NiMo/\gamma\text{-}Al_2O_3$. *Appl. Catal.*

A Gen. **2010**, *389* (1–2), 114–121.

(42) Massoth, F. E.; Politzer, P.; Concha, M. C.; Murray, J. S.; Jakowski, J.; Simons, J. Catalytic Hydrodeoxygenation of Methyl-Substituted Phenols: Correlations of Kinetic Parameters with Molecular Properties. *J. Phys. Chem. B* **2006**, *110* (29), 14283–14291.

(43) Wang, W.; Zhang, K.; Li, L.; Wu, K.; Liu, P.; Yang, Y. Synthesis of Highly Active Co-Mo-S Unsupported Catalysts by a One-Step Hydrothermal Method for p-Cresol Hydrodeoxygenation. *Ind. Eng. Chem. Res.* **2014**.

(44) Wang, W.; Li, L.; Wu, K.; Zhu, G.; Tan, S.; Li, W.; Yang, Y. MoS_2 Nanosheets and Their Hydrodeoxygenation. *RSC Advances.* **2015**, 61799–61807.

(45) Wu, K.; Wang, W.; Guo, H.; Yang, Y.; Huang, Y.; Li, W.; Li, C. Engineering Co Nanoparticles Supported on Defect MoS_{2-x} for Mild Deoxygenation of Lignin-Derived Phenols to Arenes. *ACS Energy Lett.* **2020**, *5* (4), 1330–1336.

(46) Wang, W.; Tan, S.; Wu, K.; Zhu, G.; Liu, Y.; Tan, L.; Huang, Y.; Yang, Y. Hydrodeoxygenation of P-Cresol as a Model Compound for Bio-Oil on MoS_2: Effects of Water and Benzothiophene on the Activity and Structure of Catalyst. *Fuel* **2018**.

(47) Wu, K.; Liu, Y.; Wang, W.; Huang, Y.; Li, W.; Shi, Q.; Yang, Y. Preparation of Hydrophobic MoS_2, NiS_2-MoS_2 and CoS_2-MoS_2 for Catalytic Hydrodeoxygenation of Lignin-Derived Phenols. *Mol. Catal.* **2019**, *477*.

(48) Wang, W.; Li, L.; Tan, S.; Wu, K.; Zhu, G.; Liu, Y.; Xu, Y.; Yang, Y. Preparation of NiS_2/MoS_2 Catalysts by Two-Step Hydrothermal Method and Their Enhanced Activity for Hydrodeoxygenation of p-Cresol. *Fuel* **2016**, *179*, 1–9.

(49) Tran, C. C.; Stankovikj, F.; Garcia-Perez, M.; Kaliaguine, S. Unsupported Transition Metal-Catalyzed Hydrodeoxygenation of Guaiacol. *Catal. Commun.* **2017**, *101*, 71–76.

(50) Song, W.; Zhou, S.; Hu, S.; Lai, W.; Lian, Y.; Wang, J.; Yang, W.; Wang, M.; Wang, P.; Jiang, X. Surface Engineering of CoMoS Nanosulfide for Hydrodeoxygenation of Lignin-Derived Phenols to Arenes. *ACS Catal.* **2019**, *9* (1), 259–268.

(51) Wang, W.; Li, L.; Wu, K.; Zhu, G.; Tan, S.; Liu, Y.; Yang, Y. Highly Selective Catalytic Conversion of Phenols to Aromatic Hydrocarbons on CoS_2/MoS_2 Synthesized Using a Two Step Hydrothermal Method. *RSC Adv.* **2016**, *6* (37), 31265–31271.

(52) Yoosuk, B.; Tumnantong, D.; Prasassarakich, P. Unsupported MoS_2 and $CoMoS_2$ Catalysts for Hydrodeoxygenation of Phenol. *Chem. Eng. Sci.* **2012**, *79*, 1–7.

(53) Yoosuk, B.; Tumnantong, D.; Prasassarakich, P. Amorphous Unsupported Ni-Mo Sulfide Prepared by One Step Hydrothermal Method for Phenol Hydrodeoxygenation. *Fuel* **2012**.

(54) Yang, Y. Q.; Tye, C. T.; Smith, K. J. Influence of MoS_2 Catalyst Morphology on the Hydrodeoxygenation

of Phenols. *Catal. Commun.* **2008**, *9* (6), 1364–1368.

(55) Wang, W.; Zhang, K.; Qiao, Z.; Li, L.; Liu, P.; Yang, Y. Hydrodeoxygenation of P-Cresol on Unsupported Ni-W-Mo-S Catalysts Prepared by One Step Hydrothermal Method. *Catal. Commun.* **2014**, *56*, 17–22.

(56) Wang, C.; Wang, D.; Wu, Z.; Wang, Z.; Tang, C.; Zhou, P. Effect of W Addition on the Hydrodeoxygenation of 4-Methylphenol over Unsupported NiMo Sulfide Catalysts. *Appl. Catal. A Gen.* **2014**, *476*, 61–67.

(57) Wang, C.; Wu, Z.; Tang, C.; Li, L.; Wang, D. The Effect of Nickel Content on the Hydrodeoxygenation of 4-Methylphenol over Unsupported NiMoW Sulfide Catalysts. *Catal. Commun.* **2013**, *32* (3), 76–80.

(58) Whiffen, V. M. L.; Smith, K. J. Hydrodeoxygenation of 4-Methylphenol over Unsupported MoP, MoS_2, and MoO_x Catalysts. *Energy and Fuels* **2010**, *24* (9), 4728–4737.

(59) Wang, W.; Li, L.; Zhang, K.; Qiao, Z.; Liu, P.; Yang, Y. Hydrodeoxygenation of P-Cresol on MoS_2: The Effect of Adding Hexadecyl Trimethyl Ammonium Bromide during the Catalyst Synthesis. *React. Kinet. Mech. Catal.* **2014**, *113* (2), 417–429.

(60) Wang, W.; Li, L.; Wu, K.; Zhang, K.; Jie, J.; Yang, Y. Preparation of Ni-Mo-S Catalysts by Hydrothermal Method and Their Hydrodeoxygenation Properties. *Appl. Catal. A Gen.* **2015**, *495*, 8–16.

(61) Guo, X.; Wang, W.; Wu, K.; Huang, Y.; Shi, Q.; Yang, Y. Biomass and Bioenergy Preparation of Fe Promoted MoS_2 Catalysts for the Hydrodeoxygenation of p-Cresol as a Model Compound of Lignin-Derived Bio-Oil. *Biomass and Bioenergy*. **2019**, *125*, 34–40.

(62) Joffres, B.; Nguyen, M. T.; Laurenti, D.; Lorentz, C.; Souchon, V.; Charon, N.; Daudin, A.; Quignard, A.; Geantet, C. Lignin Hydroconversion on MoS_2-Based Supported Catalyst: Comprehensive Analysis of Products and Reaction Scheme. *Appl. Catal. B Environ.* **2016**, *184*, 153–162.

(63) Zingler, M.; Martin, H.; Gabrielsen, J.; Lasse, R.; Arendt, P.; Degn, A. A Perspective on Catalytic Hydropyrolysis of Biomass. **2021**, *143*.

(64) Grilc, M.; Likozar, B.; Levec, J. Hydrodeoxygenation and Hydrocracking of Solvolysed Lignocellulosic Biomass by Oxide, Reduced and Sulphide Form of NiMo, Ni, Mo and Pd Catalysts. *Appl. Catal. B Environ.* **2014**, *150–151*, 275–287.

(65) Grilc, M.; Veryasov, G.; Likozar, B.; Jesih, A.; Levec, J. Hydrodeoxygenation of Solvolysed Lignocellulosic Biomass by Unsupported MoS_2, MoO_2, Mo_2C and WS_2 Catalysts. *Appl. Catal. B Environ.* **2015**, *163*, 467–477.

(66) Ji, N.; Diao, X.; Li, X.; Jia, Z.; Zhao, Y.; Lu, X.; Song, C.; Liu, Q.; Li, C. Toward Alkylphenols Production: Lignin Depolymerization Coupling with Methoxy Removal over Supported MoS_2 Catalyst. *Ind. Eng. Chem. Res.* **2020**, *59* (39), 17287–17299.

(67) Kumar, C. R.; Anand, N.; Kloekhorst, A.; Cannilla, C.; Bonura, G.; Frusteri, F.; Barta, K.; Heeres, H. J. Solvent Free Depolymerization of Kraft Lignin to Alkyl-Phenolics Using Supported NiMo and CoMo

Catalysts. *Green Chem.* **2015**.

(68) Narani, A.; Chowdari, R. K.; Cannilla, C.; Bonura, G.; Frusteri, F.; Heeres, H. J.; Barta, K. Efficient Catalytic Hydrotreatment of Kraft Lignin to Alkylphenolics Using Supported NiW and NiMo Catalysts in Supercritical Methanol. *Green Chem.* **2015**.

(69) Pu, J.; Nguyen, T. S.; Leclerc, E.; Lorentz, C.; Laurenti, D.; Pitault, I.; Tayakout-Fayolle, M.; Geantet, C. Lignin Catalytic Hydroconversion in a Semi-Continuous Reactor: An Experimental Study. *Appl. Catal. B Environ.* **2019**, *256*, 117769.

(70) Pu, J.; Laurenti, D.; Geantet, C.; Tayakout-Fayolle, M.; Pitault, I. Kinetic Modeling of Lignin Catalytic Hydroconversion in a Semi-Batch Reactor. *Chem. Eng. J.* **2020**, *386*, 122067.

(71) Shumeiko, B.; Auersvald, M.; Straka, P.; Šimáček, P.; Vrtiška, D.; Kubička, D. Efficient One-Stage Bio-Oil Upgrading over Sulfided Catalysts. *ACS Sustain. Chem. Eng.* **2020**.

(72) Arora, P.; Ojagh, H.; Woo, J.; Lind Grennfelt, E.; Olsson, L.; Creaser, D. Investigating the Effect of Fe as a Poison for Catalytic HDO over Sulfided NiMo Alumina Catalysts. *Appl. Catal. B Environ.* **2018**, *227*, 240–251.

(73) Wang, W.; Li, L.; Wu, K.; Zhu, G.; Tan, S.; Li, W.; Yang, Y. Hydrothermal Synthesis of Bimodal Mesoporous MoS_2 Nanosheets and Their Hydrodeoxygenation Properties. *RSC Adv.* **2015**, *5* (76), 61799–61807.

(74) Salam, M. A.; Arora, P.; Ojagh, H.; Cheah, Y. W.; Olsson, L.; Creaser, D. NiMoS on Alumina-USY Zeolites for Hydrotreating Lignin Dimers: Effect of Support Acidity and Cleavage of C-C Bonds. *Sustain. Energy Fuels* **2019**, *4* (1), 149–163.

(75) Ferdous, D.; Dalai, A. K.; Adjaye, J.; Kotlyar, L. Surface Morphology of $NiMo/Al_2O_3$ Catalysts Incorporated with Boron and Phosphorus: Experimental and Simulation. *Appl. Catal. A Gen.* **2005**, *294* (1), 80–91.

(76) Lindfors, C.; Mäki-Arvela, P.; Paturi, P.; Aho, A.; Eränen, K.; Hemming, J.; Peurla, M.; Kubička, D.; Simakova, I. L.; Murzin, D. Y. Hydrodeoxygenation of Isoeugenol over Ni- And Co-Supported Catalysts. *ACS Sustain. Chem. Eng.* **2019**, *7* (17), 14545–14560.

(77) Tieuli, S.; Mäki-Arvela, P.; Peurla, M.; Eränen, K.; Wärnå, J.; Cruciani, G.; Menegazzo, F.; Murzin, D. Y.; Signoretto, M. Hydrodeoxygenation of Isoeugenol over Ni-SBA-15: Kinetics and Modelling. *Appl. Catal. A Gen.* **2019**, *580*, 1–10.

(78) Byskov, L. S.; Nørskov, J. K.; Clausen, B. S.; Topsøe, H. DFT Calculations of Unpromoted and Promoted MoS_2-Based Hydrodesulfurization Catalysts. *J. Catal.* **1999**, *187* (1), 109–122.

(79) Fahim, M. A.; Alsahhaf, T. A.; Elkilani, A. Refinery Feedstocks and Products. *Fundam. Pet. Refin.* **2010**, 11–31.

(80) Thring, R. W.; Katikaneni, S. P. R.; Bakhshi, N. N. Production of Gasoline Range Hydrocarbons from

Alcell Lignin Using HZSM-5 Catalyst. *Fuel Process. Technol.* **2000**, *62* (1), 17–30.

(81) Lian, J.; Ma, J.; Duan, X.; Kim, T.; Li, H.; Zheng, W. One-Step Ionothermal Synthesis of γ-Al_2O_3 Mesoporous Nanoflakes at Low Temperature. *Chem. Commun.* **2010**, *46* (15), 2650–2652.

(82) Akhtar, M. S.; Riaz, S.; Mehmood, R. F.; Ahmad, K. S.; Alghamdi, Y.; Malik, M. A.; Naseem, S. Surfactant and Template Free Synthesis of Porous ZnS Nanoparticles. *Mater. Chem. Phys.* **2017**, *189*, 28–34.

(83) Han, W.; Nie, H.; Long, X.; Li, M.; Yang, Q.; Li, D. Effects of the Support Brønsted Acidity on the Hydrodesulfurization and Hydrodenitrogention Activity of Sulfided NiMo/Al_2O_3 Catalysts. *Catal. Today* **2017**, *292*, 58–66.

(84) Biesinger, M. C. Advanced Analysis of Copper X-Ray Photoelectron Spectra. *Surf. Interface Anal.* **2017**, *49* (13), 1325–1334.

(85) Vuori, A.; Bredenberg, J. B. Hydrogenolysis and Hydrocracking of the Carbon-Oxygen Bond: 5. Hydrogenolysis of 4-Propylguaiacol by Sulfided CoO-MoO_3/γ-Al_2O_3. *Holzforschung* **1984**, *38* (5), 253–262.

(86) Vuori, A.; Helenius, A.; Bredenberg, J. B. S. Influence of Sulphur Level on Hydrodeoxygenation. *Appl. Catal.* **1989**, *52* (1), 41–56.

(87) Song, S.; Zhang, J.; Yan, N. Support Effects in the De-Methoxylation of Lignin Monomer 4-Propylguaiacol over Molybdenum-Based Catalysts. *Fuel Process. Technol.* **2020**, *199*, 106224.

(88) He, Y.; Bie, Y.; Lehtonen, J.; Liu, R.; Cai, J. Hydrodeoxygenation of Guaiacol as a Model Compound of Lignin-Derived Pyrolysis Bio-Oil over Zirconia-Supported Rh Catalyst : Process Optimization and Reaction Kinetics. *Fuel* **2019**, *239*, 1015–1027.

(89) Bomont, L.; Alda-Onggar, M.; Fedorov, V.; Aho, A.; Peltonen, J.; Eränen, K.; Peurla, M.; Kumar, N.; Wärnå, J.; Russo, V. Production of Cycloalkanes in Hydrodeoxygenation of Isoeugenol Over Pt- and Ir-Modified Bifunctional Catalysts. *Eur. J. Inorg. Chem.* **2018**.

(90) Santos, J. L.; Alda-Onggar, M.; Fedorov, V.; Peurla, M.; Eränen, K.; Mäki-Arvela, P.; Centeno, M.; Murzin, D. Y. Hydrodeoxygenation of Vanillin over Carbon Supported Metal Catalysts. *Appl. Catal. A Gen.* **2018**, *561* (March), 137–149.

(91) Zhang, C.; Li, P.; Liu, X.; Liu, T.; Jiang, Z.; Li, C. General Morphology-Performance Relation of (Co) MoS_2 Catalysts in the Hydrodesulfurization of FCC Gasoline. *Appl. Catal. A, Gen.* **2018**, *556*, 20–28.

(92) Kruk, M.; Jaroniec, M. Gas Adsorption Characterization of Ordered Organic - Inorganic Nanocomposite Materials. **2001**, 3169–3183.

(93) Lin, H.; Chen, X.; Li, H.; Yang, M.; Qi, Y. Hydrothermal Synthesis and Characterization of MoS_2 Nanorods. *Mater. Lett.* **2010**, *64* (15), 1748–1750.

(94) Jagminas, A.; Niaura, G.; Žalneravičius, R.; Trusovas, R.; Račiukaitis, G.; Jasulaitiene, V. Laser Light

Induced Transformation of Molybdenum Disulphide-Based Nanoplatelet Arrays. *Sci. Rep.* **2016**, *6*, 2–10.

(95) Bremmer, G. M.; van Haandel, L.; Hensen, E. J. M.; Frenken, J. W. M.; Kooyman, P. J. The Effect of Oxidation and Resulfidation on (Ni/Co)MoS_2 Hydrodesulfurisation Catalysts. *Appl. Catal. B Environ.* **2019**, *243* (2019), 145–150.

(96) Benoist, L.; Gonbeau, D.; Pfister-Guillouzo, G.; Schmidt, E.; Meunier, G.; Levasseur, A. XPS Analysis of Oxido-Reduction Mechanisms during Lithium Intercalation in Amorphous Molybdenum Oxysulfide Thin Films. *Solid State Ionics* **1995**, *76* (1–2), 81–89.

(97) Solymosi, F.; Cserényi, J.; Szöke, A.; Bánsági, T.; Oszkó, A. Aromatization of Methane over Supported and Unsupported Mo-Based Catalysts. *J. Catal.* **1997**.